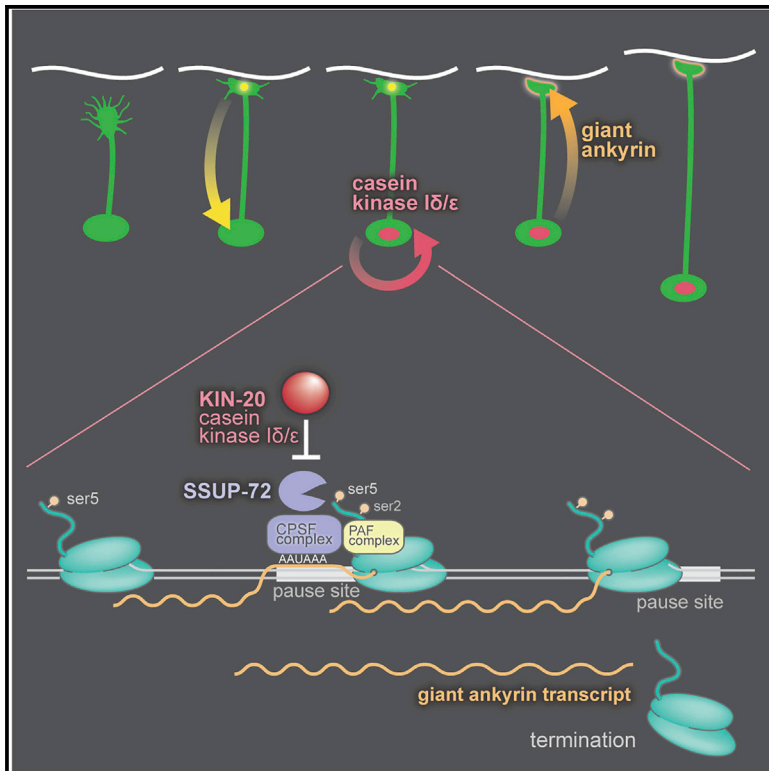


Developmental Cell

Casein Kinase 1 δ Stabilizes Mature Axons by Inhibiting Transcription Termination of Ankyrin

Graphical Abstract



Authors

Matthew L. LaBella, Edward J. Hujber, Kristin A. Moore, ..., Julie Hollien, Michael J. Bastiani, Erik M. Jorgensen

Correspondence

jorgensen@biology.utah.edu

In Brief

In *C. elegans*, casein kinase 1 delta accumulates in the nucleus after synapse formation, suppressing growth cones and stabilizing synapses and axons. LaBella et al. show that CK1 δ phosphorylates and inhibits transcription termination at a short alternative polyadenylation site within *ankyrin*, promoting expression of giant Ankyrin and stabilizing axonal growth.

Highlights

- Casein kinase 1 δ (CK1 δ) stabilizes nervous system architecture after axon outgrowth
- CK1 δ phosphorylates and inhibits SSUP-72, an RNA polymerase II CTD phosphatase
- CK1 δ inhibits transcription termination to promote giant Ankyrin expression
- Expression of giant Ankyrin in CK1 δ mutants rescues axon maturation defects



Casein Kinase 1 δ Stabilizes Mature Axons by Inhibiting Transcription Termination of Ankyrin

Matthew L. LaBella,^{1,4} Edward J. Hujber,¹ Kristin A. Moore,^{2,5} Randi L. Rawson,^{1,6} Sean A. Merrill,^{1,7} Patrick D. Allaire,^{1,8} Michael Ailion,³ Julie Hollien,² Michael J. Bastiani,² and Erik M. Jorgensen^{1,9,*}

¹Department of Biology, Howard Hughes Medical Institute, University of Utah, Salt Lake City, UT, USA

²Department of Biology, University of Utah, Salt Lake City, UT, USA

³Department of Biochemistry, University of Washington, Seattle, WA, USA

⁴Present address: Vollum Institute, Oregon Health Science University, Portland, OR, USA

⁵Present address: Renewable and Sustainable Energy Institute, University of Colorado Boulder, CO, USA

⁶Present address: Myriad Genetics, Salt Lake City, UT, USA

⁷Present address: Department of Molecular and Cellular Physiology, Stanford University, Stanford, CA, USA

⁸Present address: Center for Human Genetics, Marshfield Clinic, WI, USA

⁹Lead Contact

*Correspondence: jorgensen@biology.utah.edu

<https://doi.org/10.1016/j.devcel.2019.12.005>

SUMMARY

After axon outgrowth and synapse formation, the nervous system transitions to a stable architecture. In *C. elegans*, this transition is marked by the appearance of casein kinase 1 δ (CK1 δ) in the nucleus. In CK1 δ mutants, neurons continue to sprout growth cones into adulthood, leading to a highly ramified nervous system. Nervous system architecture in these mutants is completely restored by suppressor mutations in ten genes involved in transcription termination. CK1 δ prevents termination by phosphorylating and inhibiting SSUP-72. SSUP-72 would normally remodel the C-terminal domain of RNA polymerase in anticipation of termination. The antitermination activity of CK1 δ establishes the mature state of a neuron by promoting the expression of the long isoform of a single gene, the cytoskeleton protein Ankyrin.

INTRODUCTION

Axon guidance during nervous system development is mediated by growth cones that pioneer a pathway from the cell body to the target. When a growth cone reaches its goal, the growth cone collapses, a synapse is formed, the axon is stabilized, and the neuron acquires its mature morphology. This transition from an immature to a mature neuron must require reprogramming of the nucleus, presumably in response to interactions of adhesion molecules and the formation of a synapse. Thereafter, neuronal architecture and synaptic connectivity is maintained for the lifetime of the animal despite mechanical stress, growth, and aging of the animal. By contrast, neurons that fail to mature are marked by retraction of axons and continued sprouting of growth cones throughout the course of the animal's lifetime.

Mutants with defects in axon outgrowth superficially resemble those with defects in maturation: axons are misplaced or truncated when imaged in adult animals. However, mutants with

defects in maturation will exhibit normal axon guidance and synapse formation during development. Even demonstrating that axon outgrowth is normal during development can be inadequate. For example, mutants lacking β -spectrin exhibit normal outgrowth during development followed by continued emergence of growth cones in mature neurons in *C. elegans* (Hammarlund et al., 2000). However, ectopic growth cones arise because of axon breaks during movement and not defects in maturation. If movement is blocked in β -spectrin mutants, axon breaks are suppressed and the architecture of the nervous system is stable (Hammarlund et al., 2007). Thus, neuron maturation is normal, and growth cone sprouting is due to normal regenerative processes after axon damage in spectrin mutants.

To date, relatively few genes have been identified that play a specific role in the establishment of the mature state. Although mutations in *unc-119* in *C. elegans* display normal axon outgrowth in time-lapse imaging and form synapses, they continue sprouting growth cones into adulthood (Knobel et al., 2001). UNC-119 is a conserved protein that binds acyl groups of G-proteins (Zhang et al., 2011), but its specific binding target required to establish the mature state of the nervous system remains unknown. The cytoskeleton protein Ankyrin has also been implicated in the maintenance of axon morphology in invertebrates and vertebrates. In addition to the ubiquitous short isoforms, Ankyrins encode giant isoforms that are specifically expressed in neurons (Bennett et al., 1982; Jegla et al., 2016; Kordeli et al., 1995; Kunimoto et al., 1991). In *Drosophila*, mutants lacking the giant isoform of Ankyrin form synapses but then retract them, suggesting that there is a defect in the establishment of the mature state (Koch et al., 2008; Pielage et al., 2008). In *C. elegans*, Ankyrin mutants exhibit axon defects (Hedgecock et al., 1985; McIntire et al., 1992; Otsuka et al., 1995, 2002), and the expression of giant ankyrin in neurons is regulated by termination at an alternative polyadenylation site (Chen et al., 2015, 2017). These data suggest that UNC-119 and giant Ankyrin are structural components that establish the mature state of an axon. However, "maturation" implies that there must be a signaling pathway. Specifically, the neuron must "sense" that it has formed synapses to the correct target and reprogram its nucleus to repress outgrowth and maintain a stable architecture.



To identify new genes required for neuron maturation, we screened for mutants that continue to sprout growth cones after nervous system differentiation in *C. elegans*. We identified mutations in casein kinase 1 δ (CK1 δ /*kin-20*) that result in a massive disruption of axon morphology in the adult animal. The mutations in *kin-20* do not disrupt axon outgrowth or synapse formation during development, instead neurons continue to sprout growth cones even after development is complete, which eventually leads to a highly branched nervous system. To identify the signaling pathway downstream of CK1 δ , we performed a suppressor screen and found that CK1 δ functions to promote expression of the giant isoform of Ankyrin. The screen identified 39 mutations in 13 genes that when mutated restore nervous system stability in the CK1 δ mutant. Furthermore, second-site mutations in 10 components of the RNA polymerase-II termination complex restore expression of Ankyrin with remarkable specificity. These results suggest that CK1 δ /*kin-20* might function as a switch to stabilize mature nervous system architecture.

RESULTS

CK1 δ Is Required to Establish a Mature Nervous System Architecture

To identify genes required for the maintenance of nervous system architecture, we screened for mutants exhibiting highly branched axons in *C. elegans*. The mutation *ox423* causes animals to be dumphy and exhibit progressive paralysis, similar to β -spectrin/*unc-70* mutants. Mapping and genome sequencing demonstrated that *ox423* is a mutation in *kin-20*, which encodes the kinase CK1 δ . The CK1 δ ortholog in *Drosophila* was isolated as *doubletime*, a mutant with defects in circadian rhythms (Kloss et al., 1998; Price et al., 1998). A conserved pathway comprising *doubletime*, *period*, and *timeless* regulate circadian rhythms in most animals (Young and Kay, 2001) and regulate heterochronic gene expression in nematodes (Rhodehouse et al., 2018; Temmerman et al., 2011; Tennessen et al., 2006, 2010). In nematodes, the knockdown of *kin-20* by RNA interference promoted the formation of precocious, stage-specific cuticle structures called alae (Banerjee et al., 2005; Rhodehouse et al., 2018).

In *C. elegans*, the CK1 family includes *kin-19* (CK1 α), *csnk-1* (CK1 γ), and *kin-20* (CK1 δ); in vertebrates, a fourth homolog, called CK1 ϵ , has arisen from a duplication of CK1 δ (Fish et al., 1995). *kin-20(ox423)* contains a nonsense mutation (Q344stop) in the kinase domain (Figure 1A). A deletion allele *ok505*, obtained from the knockout consortium (*C. elegans* Deletion Mutant Consortium, 2012), exhibits an identical phenotype and fails to complement *ox423*; we conclude that they both represent null mutations. To confirm that *kin-20* is the relevant gene, we rescued the mutant with a single-copy transgene (Figure S1A). *kin-20* mutations exhibit a maternal effect, uncoordinated phenotype. Specifically, heterozygous mothers (*kin-20(ox423)/+*) produce homozygous offspring that are healthy and coordinated but slightly constipated. By contrast, offspring from homozygous *kin-20(ox423)* mothers are paralyzed, dumphy, and egg-laying defective. These phenotypes are not due to a strict maternal effect since they exhibit paternal rescue; *kin-20/+* offspring generated by crossing a wild-type male to a *kin-20(-)* mutant mother are grossly wild-type. Thus, either a paternal chromosome or gene products from the maternal germline are sufficient for normal development.

The nervous system in *kin-20* mutants is highly disorganized in late-larval-stage animals compared with wild-type animals (Figures 1B and 1C). During normal development, the DD GABA motor neurons extend axons from the ventral nerve cord to the dorsal nerve cord during embryogenesis, and the VD GABA motor neurons extend axons during the late L1 stage; thereafter, the architecture of the nervous system remains stable. In *kin-20* mutants, the motor neurons exhibit extra commissures, misrouted or branched axons, persistent growth cones, and spindly axons. To determine whether these defects arise during axon elongation or in mature neurons, we characterized the development of DD and VD motor neurons. We quantified the presence of supernumerary branches, ectopic growth cones, and thin, spindly axons during all larval stages and adults (Figures 1D–1F). Axon defects accumulate in *kin-20(ox423)* mutants as the animal ages: ectopic growth cones sprouting from the axon or cell body increased from 0.2 per animal in the L2 larval stage to 6.4 in the adult (Figure 1D). The increase in ectopic growth cones gave rise to a concomitant increase in ectopic branches, which increased from 3 branched axons per animal in the L2 stage to 24 branched axons in the adult (Figure 1E). These data suggest that the disorganized nervous system in *kin-20* mutants is caused by axon sprouting in larvae and adults.

CK1 Is Not Required for Axon Guidance or Synapse Formation

To determine if CK1 δ is required for axon outgrowth during the initial formation of the nervous system, we performed time-lapse confocal microscopy during the late L1 to L2 transition (Figures 2A and 2B; Videos S1 and S2). We monitored outgrowth by imaging VD motor neurons. VD motor neurons are born in the late L1 larval stage on the ventral side and extend growth cones to the dorsal cord during the L1 to L2 molt (Knobel et al., 1999). In *kin-20* early L2 larvae, growth cones from the VD neurons extend from the ventral to dorsal nerve cord with no signs of ectopic branching. These data suggest that axon outgrowth is normal and that branching occurs after the growth cones have reached their targets.

To monitor axon stability, we imaged DD motor neurons. The DD motor neurons are born on the ventral side and differentiate during embryogenesis; by the L1 stage, fully extended commissures are present (White et al., 1978, 1986). In *kin-20* mutants, the DD commissures are largely normal in L1 larvae: 78% of DD commissures are composed of a single unbranched axon. However, 17% of DD axons generate an interstitial growth cone, which migrates within the existing axon shaft and terminalizes in the dorsal nerve cord (Figure 2C; Video S3). The formation of interstitial growth cones is occasionally accompanied by retraction of the distal portion of the axon and re-extension along the dorsal cord by the new growth cone (Figure 2D; Video S4). In the early L2 larvae, ectopic growth cones are observed sprouting from the side of the axon shaft of DD neurons and extending toward the dorsal nerve cord (Figure 2B; Video S2). We conclude that *kin-20* mutant animals exhibit normal axon outgrowth but fail to repress the emergence of new growth cones after reaching their target.

CK1 δ Is Required for Neuronal Maturation

Growth cones continue to sprout from existing axon shafts even in late larvae and adults in CK1 δ mutants (Figure 2E; Video S5).

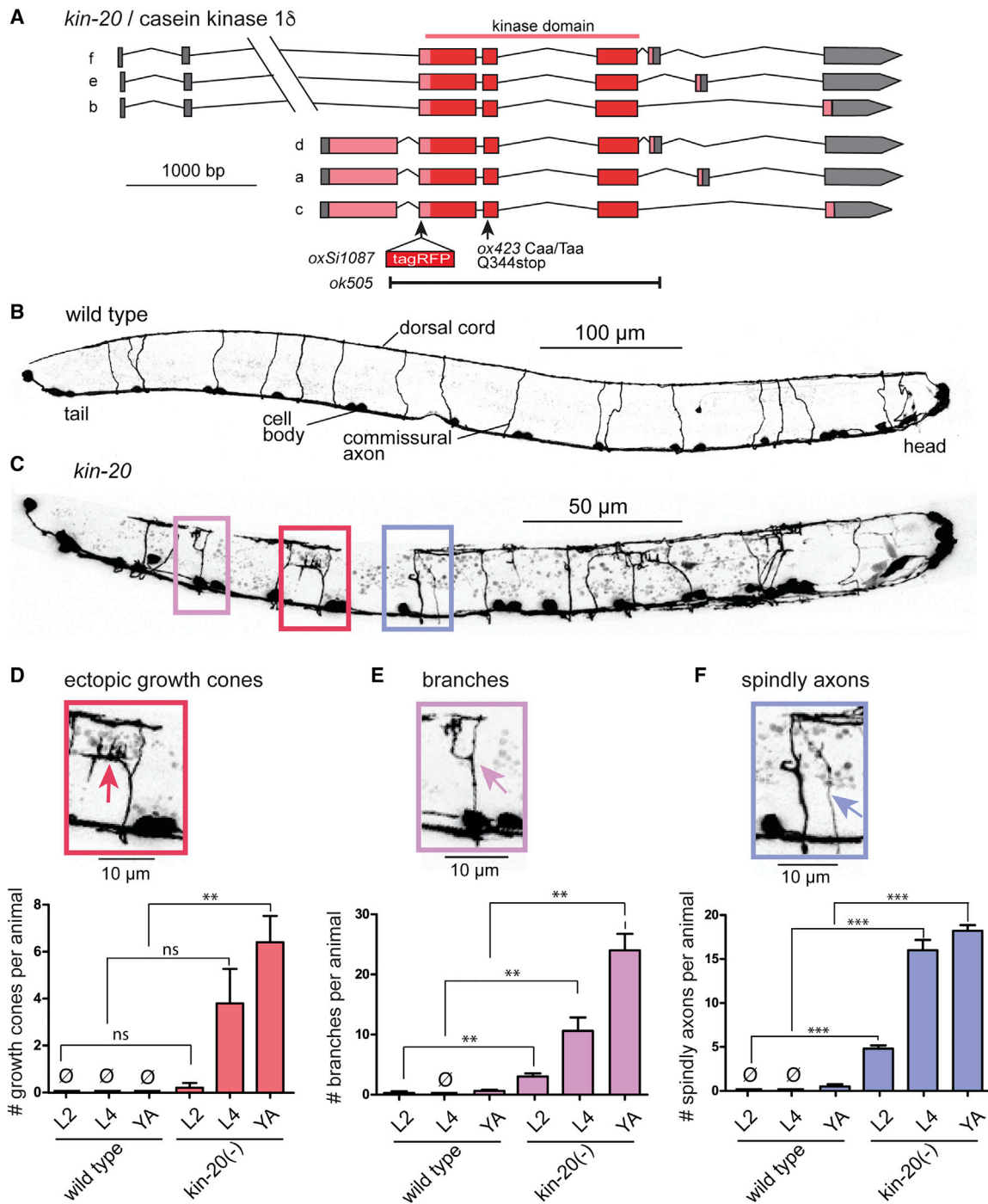


Figure 1. CK1δ Is Required to Stabilize Neuronal Architecture

(A) The *C. elegans kin-20* gene locus. The *ox423* allele is a nonsense mutation changing glutamine to a premature stop codon (KIN-20a Q344X) in the middle of the conserved kinase domain (KHQHI → KHXHI). The large 5' exon is only found in *Caenorhabditis*.

(B) Wild-type L4 larva expressing GFP in GABA DD and VD neurons (strain EG1285). Fluorescence in all images is inverted to improve the visibility of the processes.

(C) The nervous system in a mature *kin-20* mutant is highly disorganized. A *kin-20(ox423)* L4 larva expressing GFP in all GABA neurons (EG5202). Boxes show examples of structures quantified in (C)–(E).

(D–F) (D) Ectopic growth cones, (E) branches, and (F) spindly axons (mean ± SEM per animal) in larval stages L2, L4, and young adults (YAs) (number scored axons is ≥ 80, Welch's t test: *p < 0.05, **p < 0.01, ***p < 0.001, ns p > 0.05).

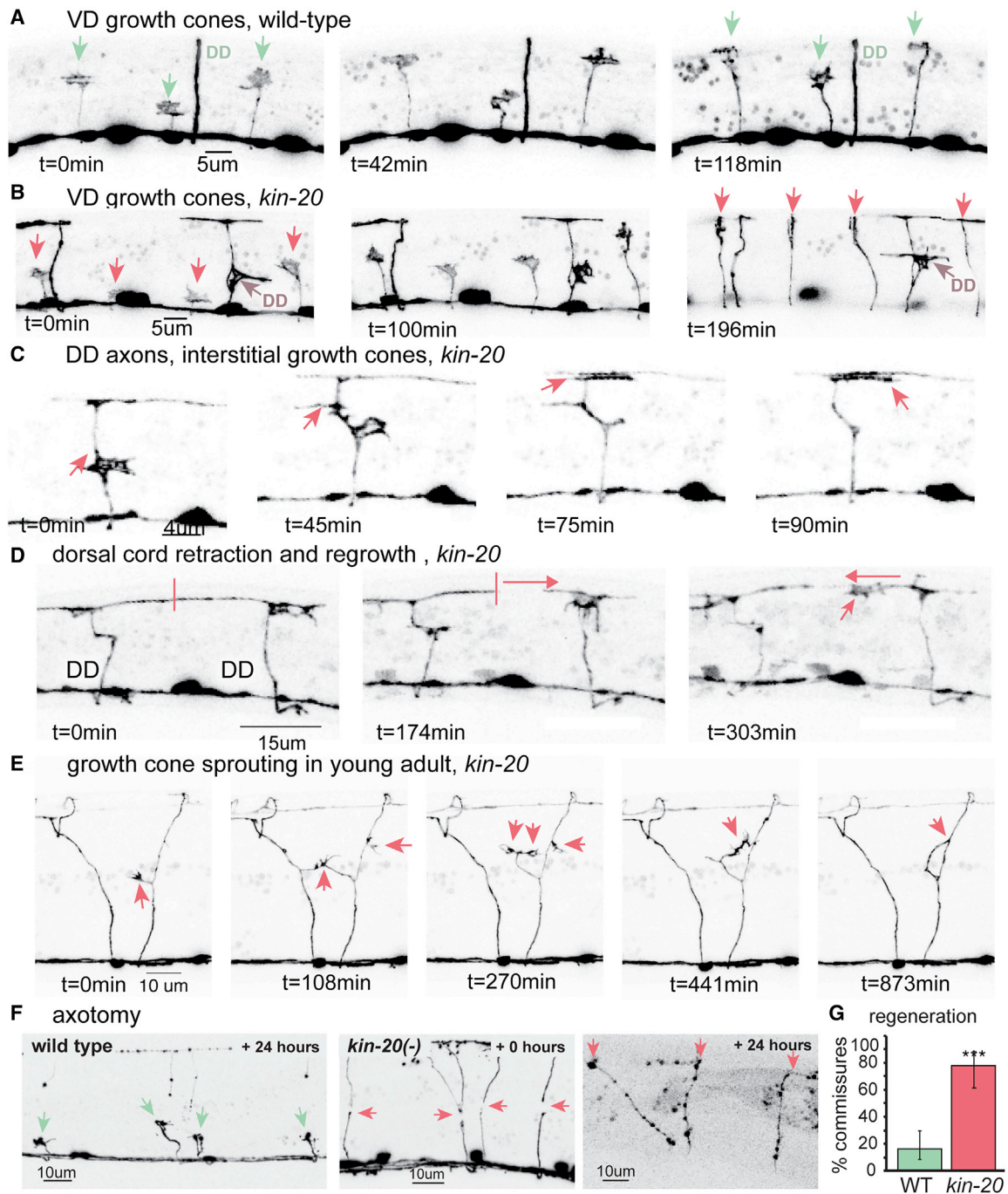


Figure 2. CK1 δ Is Required for Neuronal Maturation, Not Axon Guidance

(A) Wild-type VD growth cones (arrows) extend during the early L2 larval stage (EG1285). The DD axon has already extended and formed neuromuscular junctions during embryogenesis.

(B) Primary VD growth cones extend normally in *kin-20* larvae (EG5202).

(C) Mature neurons continue to extend growth cones in *kin-20* mutants. An interstitial growth cone extends within a differentiated DD axon shaft and terminalizes in the dorsal nerve cord.

(D) The dorsal cord retracts (panel 2), and the secondary growth cone extends into the synaptic region in a *kin-20* mutant.

(E) Growth cones sprout continuously from commissures in older *kin-20* larvae and adults; in this example, the growth cone fuses with its own axon and collapses.

(F) CK1 δ inhibits regeneration. Left: most cut axons (green arrows) in the wild type remain as stalled growth cones or stumps 24 h after axotomy. Middle: in *kin-20* mutants growth cones rapidly sprout from cut axons immediately after laser axotomy (red arrows). Right: 24 h later, these same axons have reached the dorsal cord (red arrows).

(G) Following laser axotomy, growth cones reach the dorsal cord more frequently in *kin-20* mutants than in the wild type (WT 16%; *kin-20(ox423)* 78%; Fisher's exact test *** $p < 0.01$, error bars represent 95% CI, $n > 100$).

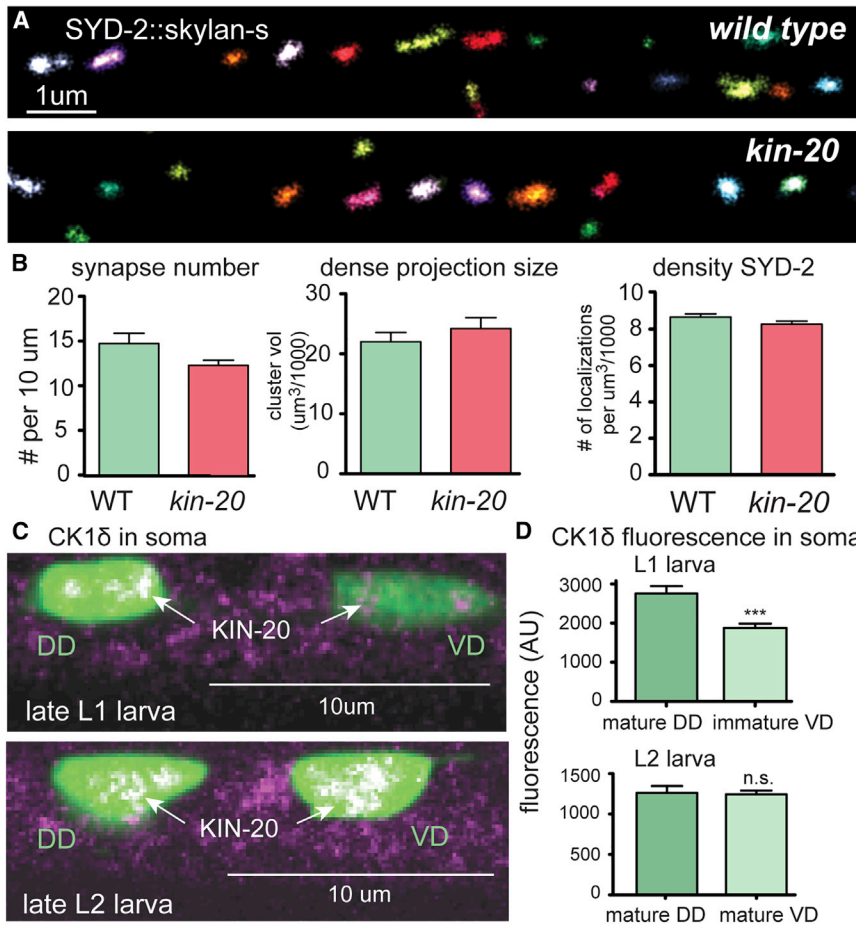


Figure 3. CK1 δ Localizes to Neuron Cell Bodies during Synapse Formation

(A) Synapse formation is normal in *kin-20* mutants. Super-resolution imaging of liprin- α /SYD-2 tagged with Skylan-S along the ventral cord of wild-type and *kin-20(-)* L2 larvae (EG9812 and EG9811, respectively). Colors distinguish individual clusters. (B) Synapses are normal for the number of SYD-2 labeled synapses ($p = 0.85$), volume of SYD-2 dense projections ($p = 0.36$, unpaired t test), and SYD-2 protein density ($p = 0.12$) (see Figure S2 for RIMB-1 and NRX-1 data, number of scored synapses is > 120). (B&D) comparisons by unpaired t test, error bars represent \pm SEM.

(C) CK1 δ (tagRFP) is observed in cell bodies of mature DD neurons in late L1 animals but not in cell bodies of immature VD neurons (top). Tagged CK1 δ also appears in cell bodies of VD neurons after synapse formation in the late L2 stage (bottom). (EG9581).

(D) Tagged CK1 δ fluorescence in VD cell bodies is significantly lower than in DD cell bodies in L1s (** $p < 0.001$). CK1 δ expression level is not significantly different in VD neurons after axon extension and synapse formation (ns, $p = 0.8$) (bottom).

Ectopic growth cone formation in late larvae and adult stages is also observed in β -spectrin mutants (Hammarlund et al., 2007). In β -spectrin mutants, ectopic growth cone formation is caused by axon breakage during movement; these ectopic growth cones can be fully suppressed by paralyzing the animal. To determine if ectopic growth cones were caused by movement-induced axon breaks in CK1 δ mutants, we paralyzed animals by knocking down the muscle gene Titin-related/*unc-22* using RNA interference. Chronic paralysis rescued nervous system architecture in spectrin mutants but failed to eliminate ectopic growth cone formation and axonal branching in CK1 δ mutants (Figure S1B). These data suggest that the defects in CK1 δ mutants are not because of mechanical stress to the axon but rather appear to be a defect in maturation of the axon to a stable differentiated state.

Another explanation for the CK1 δ outgrowth phenotype is that the neurons never mature. To determine whether neurons are chronically immature in *kin-20* mutants, we assayed the regenerative capacity of neurons. In *C. elegans*, young neurons regenerate better than older neurons after laser axotomy (Byrne et al., 2014; Gabel et al., 2008; Hammarlund et al., 2009; Nix et al., 2011; Wu et al., 2007; Zou et al., 2013). We cut axons in the L4 stage and assayed regeneration 24 h later. Most axons retracted or remained as persistent stumps both in the wild-type and *kin-20* mutants (Figure S1C, WT, 53%; *kin-*

mutants, similar to young animals, can regenerate cut axons better than the wild-type.

Axons may be unstable in CK1 δ mutants because they fail to recognize their targets and form synapses, and the nucleus is not reprogrammed to become a fully differentiated neuron. To determine if synapse formation was normal, we tagged three synaptic proteins, liprin- α (SYD-2), neuexin (NRX-1), and RIM-binding protein (RIMB-1) with Skylan-S using CRISPR. Synapses in the ventral nerve cord were imaged using super-resolution microscopy during the L2 larval stage before the nervous system sprouted supernumerary growth cones (Figure 3A). The number, volume, and density of the presynaptic puncta for these proteins were normal in *kin-20* mutants (Figures 3B and S2A–S2F). Thus, persistent axon outgrowth in CK1 δ mutants is not because of a failure to form synapses.

CK1 δ Acts Cell Autonomously after Axon Outgrowth and Synapse Formation

To determine in which tissue *kin-20* acts to stabilize neurons, we selectively expressed KIN-20 in the epidermis, muscle, intestine, and nervous system in *kin-20(ox423)* mutants (Table S1). Only expression of KIN-20 in neurons rescued the uncoordinated and axon branching phenotypes (Figure S3A), demonstrating that CK1 δ acts cell autonomously to stabilize neuronal architecture.

To determine the expression pattern and localization of CK1 δ , we fluorescently tagged the protein with tagRFP (Figure 1A). During embryogenesis, expression of KIN-20 is absent in early embryos but increases at the 3-fold stage and is observed as a few dim speckles in the nuclei of developing DD motor neurons (Figures S3D and S3E). In L1 hatchlings, expression is dim throughout the animal, but KIN-20 can be observed in the nuclei of neurons (Figure S3F). The VD neurons send out growth cones post-embryonically during the L1-L2 molt (Knobel et al., 1999), and during axon extension, expression in the VDs is lower than that in DD neurons (Figures 3C, 3D, and S3G). At the mid-L2 stage, the VD neurons form synapses (Hallam and Jin, 1998; Kurup and Jin, 2015; Sulston, 1976), and KIN-20 expression is identical in DD and VD cell bodies (Figures 3C and 3D). At the L2 stage, KIN-20 is also highly expressed in the nuclei of epidermal cells and is visible in the nuclei of motor neurons (Figure S3H). Expression tends to peak at the end of each larval stage, consistent with expression of other heterochronic genes (Rhodehouse et al., 2018). In the L4 stage, *kin-20* is localized to the nucleus of all cell types (Figure S3B) and at adherens junctions in the spermatheca (Figure S3C). Ubiquitous expression is consistent with CK1 δ expression in other organisms (Knippschild et al., 2005). Together, these data suggest that appearance of KIN-20 in the nuclei of neurons coincides with axon outgrowth and the formation of synapses just preceding the maturation of the nervous system.

CK1 δ Suppressors Rescue Axonal Defects

To characterize the genetic pathway downstream of *kin-20*, we performed a suppressor screen using the chemical mutagen ENU (*N*-ethyl-*N*-nitrosourea). To identify strong suppressors, we performed a multigenerational fitness screen (Hollopeter et al., 2014). We isolated 44 independent suppressor strains that were healthy and exhibited normal locomotion (Figures 4A, 4D, and S4A). Analysis of the GABA motor neurons revealed rescue of the *kin-20* neuronal branching defect in all suppressors (Figure 4E). We were able to characterize suppressor mutations in 39 of the strains comprising mutations in 13 genes (Tables 1 and S2).

Suppressors Prevent Premature Termination of Ankyrin Transcripts

We identified CK1 δ suppressor mutations by mapping them against a set of integrated fluorescence markers (Frøkjær-Jensen et al., 2014), whole-genome resequencing, and *in silico* complementation tests (Minevich et al., 2012). Most single-hit genes were validated by CRISPR; other genes were validated by transgene rescue (Table S3). Among the 39 characterized suppressors were 4 intracodon revertants of the nonsense mutation, suggesting the screen was approaching saturation. We also recovered a *kin-20* suppressor mutation in the related *kin-19* gene, which encodes casein kinase 1 alpha (Tables 1 and S2). The suppressor KIN-19(L300F) is a missense mutation in a residue at the C terminus that is conserved in all CK1 isoforms. Casein kinase isoforms are known to function redundantly in some pathways (Knippschild et al., 2005); therefore, it is likely that this mutation leads to a promiscuous or constitutively active CK1 α that compensates for the loss of CK1 δ .

Among the remaining suppressors were 30 missense mutations in 10 RNA Polymerase II subunits: *rpb-2*, *pinn-1*, *ssup-72*, *cpsf-4*, *pfs-2*, *cdc-73*, *ctr-9*, *zfp-3*, *pct-11*, and *cdk-8* (Tables 1 and S1). The suppressor mutations can be divided into five classes: RNA polymerase B catalytic subunit, RNA polymerase C-terminal domain (CTD) modifiers, cleavage and polyadenylation specificity factor (CPSF) complex, Paf1 complex (Paf1C), and Mediator complex. Each of these proteins and their associated complexes are implicated in alternative polyA site selection and transcription termination, with the exception of *cdk-8*, which functions in transcription initiation via Mediator (Allen and Taatjes, 2015; Shilatifard, 2012). These results suggest that CK1 δ acts to inhibit transcription termination at loci important for maintaining the nervous system; in the absence of CK1 δ , premature termination occurs. Premature termination at these loci can be suppressed by secondary defects in termination.

CK1 δ Phosphorylates SSUP-72

Because CK1 δ is upstream of the RNA polymerase II termination complex, it is possible that one or more proteins in the complex are phosphorylation targets of CK1 δ . SSUP-72 is a particularly interesting potential target. SSUP-72 removes the phosphate from Ser5 of the CTD of the RNA polymerase 1 subunit, and this dephosphorylation marks RNA polymerases that are approaching a termination site (Hsin and Manley, 2012; Kuehner et al., 2011). SSUP-72 was also identified previously as a regulator of alternative polyadenylation during neuron development (Chen et al., 2015). The SSUP-72 S39F suppressor mutation we identified is at a conserved S/T from yeast to humans (Figures 4B and S4B), which is in a consensus CK1 phosphorylation site (p[S/T]xx[S/T]). Phosphorylation of the first S/T residue primes CK1 δ phosphorylation of the second S/T (Knippschild et al., 2005).

To determine if SSUP-72 can be phosphorylated by CK1 δ , recombinant *C. elegans* SSUP-72 was used as a target in an *in vitro* phosphorylation assay. We found that truncated rat CK1 δ is able to phosphorylate SSUP-72 directly (Figure 4B). If SSUP-72 S39 is phosphorylated by CK1 *in vivo* to inhibit transcription termination, we would expect an SSUP-72 S39E phosphomimetic mutation would suppress the *kin-20* null phenotype. The SSUP-72(S39E) allele was generated by CRISPR and crossed into the *kin-20* null. *ssup-72(S39E)* suppressed the *kin-20* null phenotype, restoring motility to these animals (Figures 4C and 4D). The phosphorylation-defective allele *ssup-72(S39A)* did not rescue *kin-20* null animals (Figures 4C and 4D). These data demonstrate that SSUP-72 S39 is likely a key CK1 δ phosphorylation target in this axon stabilization pathway. If SSUP-72 were the sole target of CK1 δ , the *ssup-72(S39A)* mutant animals should phenocopy *kin-20* null animals. However, the *ssup-27(S39A)* animals look and behave similar to the wild type (Figures 4C and 4D). Thus, SSUP-72 phosphorylation by CK1 δ is sufficient but not necessary for the stabilization of axons, suggesting that SSUP-72 is not the sole target of CK1 δ .

CK1 δ Promotes Expression of the Giant Ankyrin Isoform

In addition to the mutations in RNA polymerase II termination subunits, we identified four suppressor mutations that disrupt termination at an early polyadenylation site in the *unc-44*

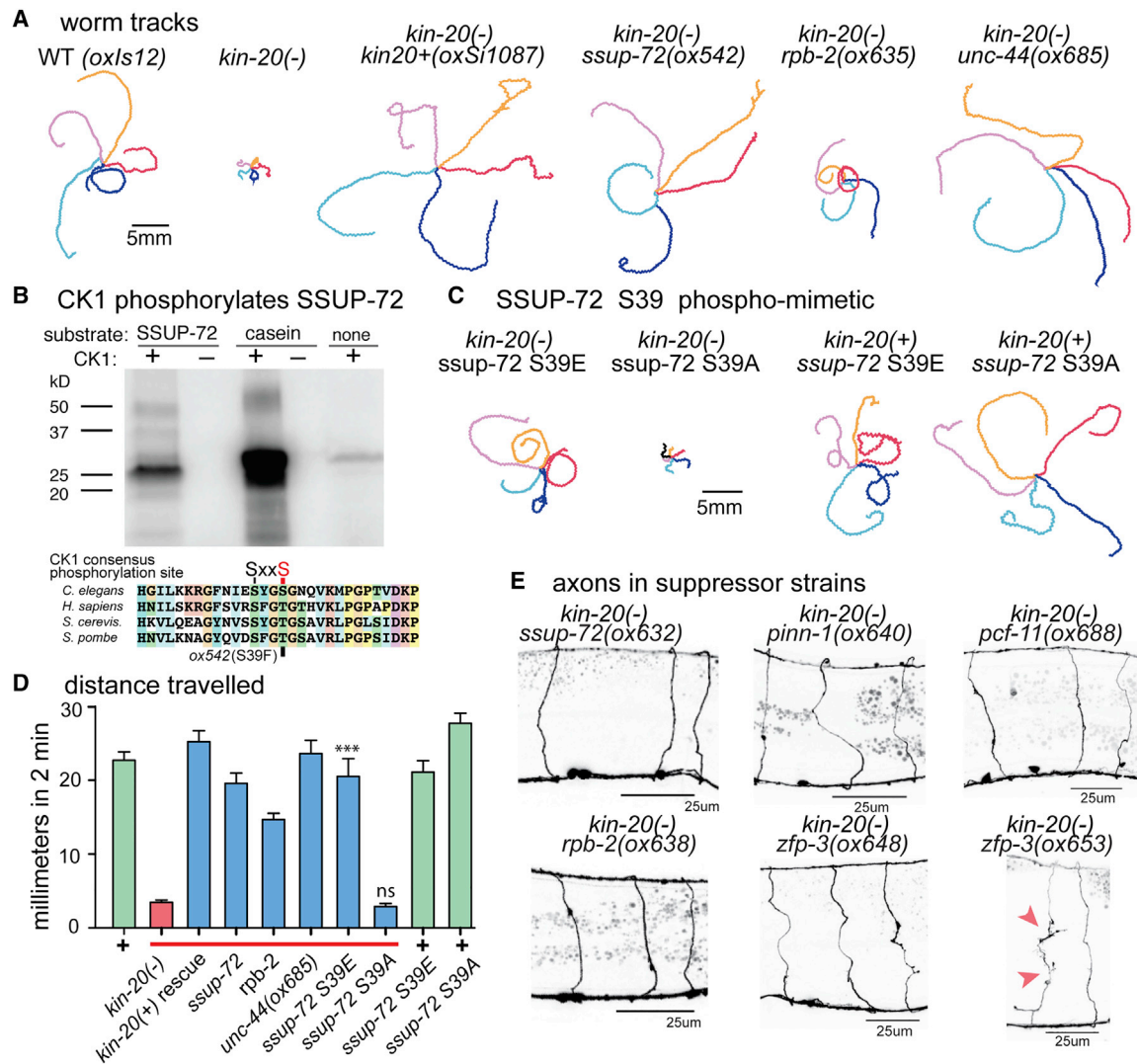


Figure 4. CK1 δ Acts on Transcription Termination

(A) Suppressors restore locomotion to *kin-20(ox423)* mutants. Worm tracks for 5 worms were imaged for 2 min and traced (for other suppressors, see Figure S4). (B) Above: CK1 δ phosphorylates SSUP-72 in an *in vitro* phosphorylation assay. Rat CK1 δ 1 was added to recombinant SSUP-72. Left, phosphorylated SSUP-72 (predicted MW 22.8 kDa); middle, phosphorylation control of phospho-primed casein; and right, CK1 δ autophosphorylation. Below: a consensus CK1 δ phosphorylation site is conserved from yeast to humans in Ssu72 orthologs. The target serine is mutated in the suppressor *ssup-72(ox542)*.

(C) The phosphomimetic mutation of SSUP-72 S39 is sufficient to suppress *kin-20* locomotory defects. Specific mutations in *ssup-72* were generated by CRISPR. (D) Quantification of distances traveled in 2 min (\pm SEM, $n = 5$). SSUP-72 S39E rescues *kin-20(ox423)* motility (** $p < 0.001$ Welch's t test) and SSUP-72 S39A does not rescue (ns, $p > 0.05$) (EG9899 and EG9914). SSUP-72 S39E and S39A mutants alone are behaviorally wild type (EG9900 and EG9913). Because SSUP-72 S39A does not phenocopy the *kin-20* null, this suggests that there are other targets of CK1 δ . SSUP-72 S39A exhibits slightly increased motility compared with the wild type ($*p < 0.05$, EG9913).

(E) *kin-20(ox423)* suppressors rescue axon defects. Some suppressors, for example, *zfp-3(ox653)*, exhibit occasional, remaining defects.

gene. *unc-44* encodes Ankyrin, a component of the spectrin cytoskeleton (Otsuka et al., 1995). *unc-44* generates three isoforms, one short, one medium, and one very long isoform, each of which uses a different polyadenylation site (Figures 5A and S5A). The long form of UNC-44 is related to the giant isoforms of Ankyrin expressed in the neurons of all bilaterians (Jegla et al., 2016). The long isoform of UNC-44 is repressed in other tissues; for example, the kinase DAPK-1 inhibits expression of the long form of Ankyrin in the epidermis of *C. elegans* (Chen et al., 2017), but it is unclear how long Ankyrin is activated in neu-

rons. Three of our suppressors are mutations in the AATAAA polyadenylation signal that generates the transcript for one of the short isoforms (Figure 5A). A fourth variant, *unc-44(ox686)*, is in the intron immediately upstream of this polyadenylation site in an adenine-rich sequence conserved in nematodes (Figures 5A and S5A). This mutation caused skipping of the downstream exon and constitutive splicing in-frame to the giant exon of the long isoform. The medium isoform controlled by polyA site #2 is not detectable by qPCR in the *unc-44(ox686)* suppressor (Figure S6B). These mutations in *unc-44* suggest

Table 1. CK1 δ Suppressors Are in Transcription Termination Components and *unc-44*/Ankyrin

Gene	Number of Alleles	Cellular Process	Mutation
<i>kin-20</i>	4	casein kinase 1 delta	missense, revertants
<i>kin-19</i>	1	casein kinase 1 alpha	missense
<i>ssup-72</i>	5	phosphatase for RNAP II CTD	missense
<i>pinn-1</i>	3	prolyl isomerase for RNAP II CTD	missense and null
<i>pcf-11</i>	1	3' pre-mRNA processing	missense
<i>cpsf-4</i>	3	cleavage polyadenylation factor complex	missense
<i>pfs-2</i>	1	cleavage polyadenylation factor complex	missense
<i>ctr-9</i>	3	elongation-termination, Paf1 complex	missense
<i>cdc-73</i>	1	elongation-termination, Paf1 complex	splice acceptor and null
<i>zfp-3</i>	7	likely RNA pol II complex	missense and nulls
<i>rpb-2</i>	5	RNAP II subunit B	missense
<i>cdk-8</i>	1	Mediator and RNA pol II complex	missense
<i>unc-44</i>	4	Ankyrin, cytoskeletal	missense
Unconfirmed Hits			
<i>zfp-3</i>	1	likely RNA pol II complex	intronic mutation
<i>swd-2.2</i>	1	Set1-COMPASS complex	missense
<i>pinn-1</i>	1	prolyl isomerase for RNAP II CTD	intronic mutation

The genes identified in the *kin-20* suppressor screen. Four *kin-20(ox423)* revertants and pseudo-revertants were identified, indicating that the screen was approaching saturation. *kin-19(ox689)* is a predicted hypermorphic mutation of casein kinase 1 α , a CK1 isoform closely related to CK1 δ . *unc-44* alleles are found in the polyadenylation site (*ox685*, *ox832*, and *ox833*) and within a conserved intron upstream of the polyadenylation site (*ox686*). All other mutations are in components of the RNA polymerase II complex, most with functions in transcription termination. The same mutation, *pfs-2(R158Q)*, was identified previously in a neuronal branching suppressor screen (Van Epps et al., 2010).

that CK1 δ suppressors promote the specific expression of the long form of Ankyrin.

In the simplest model, CK1 δ inhibits transcription termination at the polyA site #2 of *unc-44* and promotes expression of giant Ankyrin; in the absence of CK1 δ , the giant Ankyrin isoform is not expressed. In *kin-20* suppressors, transcription termination at polyA site#2 is reduced in neurons, and giant Ankyrin is restored. If this model is correct, (1) giant Ankyrin should be absent in the CK1 δ null mutant, (2) giant Ankyrin should be restored in the suppressor mutants, and (3) expression of the giant Ankyrin should rescue CK1 δ mutant animals.

To determine whether giant Ankyrin is absent in the CK1 δ mutant, we performed quantitative RT-PCR. Compared with wild-type embryos, the *unc-44* long isoform was decreased approximately 16-fold in *kin-20* mutant embryos (Figure 5B). The short and medium *unc-44* isoforms were detected at wild-type levels in *kin-20* mutant animals, indicating that the long isoform contributes little to the total level of *unc-44* mRNAs (Figure S5A for primer locations, Figures S6A and S6B). We conclude that giant Ankyrin is specifically depleted in CK1 δ mutants.

To determine if the suppressors restore giant Ankyrin transcripts, we performed qPCR on ten *kin-20* suppressor strains (Figure 5B). In all strains tested, expression of the giant Ankyrin isoform was significantly increased relative to *kin-20(ox423)*. The expression of both the short isoforms of Ankyrin remained constant in all strains except the exon-skipping mutation *unc-44(ox686)*, which lacked the short isoform controlled by polyA site #2 (Figures S6A and S6B). Because the giant Ankyrin transcript is restored in all suppressors, it is likely that the function of CK1 δ is to drive expression of the long isoform of Ankyrin.

If CK1 δ mutants have unstable axons because they lack giant Ankyrin, then expressing giant Ankyrin in the CK1 δ mutants should bypass the requirement for the kinase. We overexpressed the giant isoform of *unc-44* from an extrachromosomal array in *kin-20(ox423)* animals (Figure S5B). The axon morphology of VD and DD motor neurons in the *kin-20* mutant was rescued by *unc-44*-long overexpression (Figures 5C and 5D). The numbers of supernumerary branches, ectopic growth cones, and spindly axons in *kin-20* mutants were greatly reduced, although not completely rescued (Figure 5C). The suppressor mutation in the AAUAAA polyadenylation signal (*unc-44(ox685)*) rescued branching and spindly axon defects, but ectopic growth cones persisted (Figure 5C). The exon-skipping suppressor (*unc-44(ox686)*) fully rescued the *kin-20* axon phenotype (Figure 5C). This suppressor expresses the short and long isoforms but not the medium isoform (Figures 5C, S6A, and S6B). These data demonstrate that the major defect in CK1 δ mutant neurons is the lack of giant Ankyrin.

It is surprising that the most critical target for CK1 δ is termination at a single polyA site in the Ankyrin gene. To more fully survey the transcriptome, we performed RNA sequencing (RNA-seq) on the wild-type, *kin-20(ox423)* null animals, and *kin-20* strains with suppressor mutations (*ssup-72(ox542)* and *cpsf-4(ox649)*). The only transcript with significantly reduced expression in the *kin-20* mutant is the long form of Ankyrin (Table S4; adjusted $p < 0.1$) and levels were restored in the suppressed strains. In addition, transcripts from the non-coding RNA transcribed telomeric sequence (*tts-1*) (Essers et al., 2015) were significantly increased in *kin-20* mutants, but transcript levels of *tts-1* were not restored in the suppressor mutants, suggesting that changes in *tts-1* may be due to other targets of CK1. To

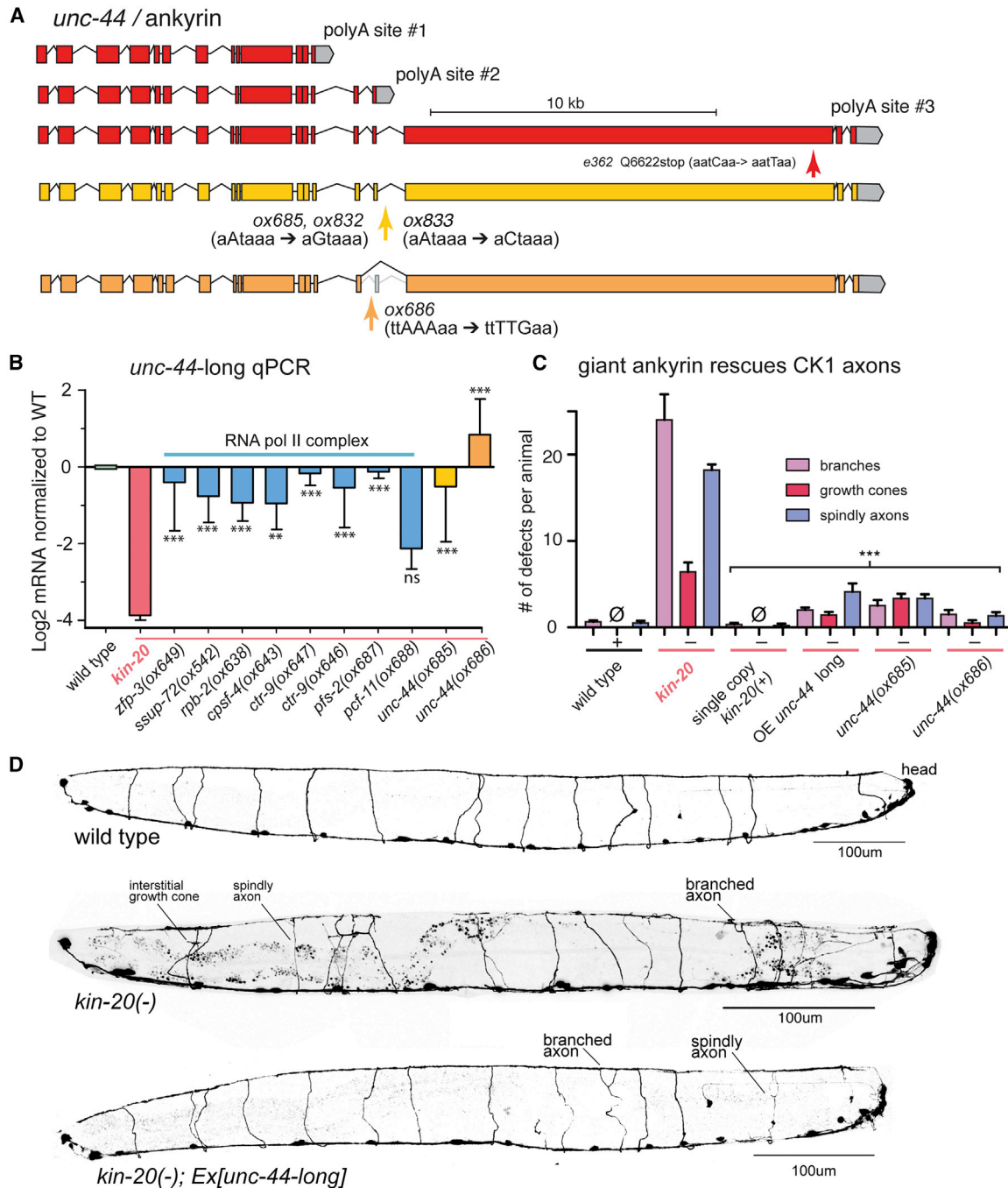


Figure 5. CK1 δ Stabilizes Mature Axons by Upregulating Giant Ankyrin Transcription

(A) Ankyrin gene model. *C. elegans* has three alternative polyA sites. Expression of the giant isoform requires readthrough at polyA site #2. Yellow; *kin-20* suppressors *unc-44*(ox685), *unc-44*(ox832), and *unc-44*(ox833). These mutations disrupt the polyA motif and likely disrupt termination. Orange, *kin-20* suppressor *unc-44*(ox686) (EG9097). The mutation is upstream of polyA site #2 in the preceding intron, which causes exon skipping, and only giant ankyrin is transcribed.

(B) *kin-20*(ox423) lacks mRNA for the giant isoform of ankyrin. qPCR of the giant isoform of *unc-44* mRNA in *kin-20*(ox423) and suppressed animals. mRNA levels are normalized to the wild type. In *kin-20* mutants, the giant isoform of *unc-44* is decreased ~16-fold compared with wild-type levels, ****p* < 0.001. All suppressors exhibited increased levels of *unc-44* mRNA compared with *kin-20*(ox423) alone, with the exception of *pcf-11*(ox688) (Dunnett's test **p* < 0.05, ***p* < 0.01, ****p* < 0.001, error bars represent \pm SEM).

(C) Quantification of axon morphology of CK1 δ mutant rescue by expression of giant ankyrin. Single-copy expression of the wild-type *kin-20* allele, *oxSi1087*, in *kin-20* null animals fully rescues axon stability. Axon defects of *kin-20*(ox423) animals are rescued by expression of a chimeric copy of *unc-44* in which the polyadenylation site #2 has been replaced by cDNA on an extrachromosomal array (EG9248, ****p* < 0.001). Both the *unc-44*(ox685) and *unc-44*(ox686) suppressor mutation rescues CK1(-) (***p* < 0.001). Mean ectopic growth cones, branches, and spindly axons were scored per adult animal. Number of scored axons

(legend continued on next page)

verify that *unc-44* is the sole target and that our RNA-seq data are correct, candidate genes were selected based on the presence of alternative polyA sites as well as genes with known roles in axon and synapse stability (Table S5). None of these candidates are differentially expressed in *kin-20(ox423)* compared with the wild type (Figure S6C). Taken together, these data demonstrate that the interaction between CK1 δ and giant Ankyrin is remarkably specific.

DISCUSSION

Mutations in *kin-20*, which encodes CK1 δ , result in a destabilized nervous system. CK1 δ null axons grow out normally and form synapses but continue to sprout growth cones and send new axons to synaptic targets. By adulthood, essentially all axons are highly branched, with many extending active growth cones, and the animals are paralyzed. To determine the pathway downstream of CK1 δ , we performed a genetic screen for suppressors. The mutations fall into two major classes: most are in genes implicated in transcription termination and polyadenylation, and the remainder disrupt the alternative polyadenylation site that precedes the long exon of giant Ankyrin. Overexpressing giant Ankyrin rescues CK1 δ null animals, demonstrating that expression of giant Ankyrin is the primary target of CK1 δ for stabilizing axons in mature neurons.

Giant Ankyrin Mediates Axon Stability

Typically, there are two types of Ankyrins expressed in bilaterians: a short and a long isoform (Jegla et al., 2016). In *C. elegans*, these isoforms are generated by alternative polyadenylation sites from a single gene *unc-44*. In *Drosophila*, there are two Ankyrin genes *Ank* and *Ank2*; *Ank* only expresses a short isoform, whereas *Ank2* expresses short, medium, long, and extra-long isoforms. Vertebrate genomes contain three Ankyrin genes, *ANK1*, *ANK2*, and *ANK3* (which encode the proteins AnkR, AnkB, and AnkG). AnkR only expresses a short isoform; AnkB and AnkG express both short and long isoforms.

Short isoforms of Ankyrin are expressed ubiquitously and are composed of 24 Ankyrin repeats, two ZU5 domains, a UPA domain, and a DEATH domain (Bennett and Lorenzo, 2013). The Ankyrin repeat domain binds transmembrane proteins including ion channels, transporters, and adhesion molecules such as L1CAM (Koenig and Mohler, 2017). The Ankyrin ZU5-UPA domain links transmembrane proteins to the spectrin cytoskeleton and transport vesicles to dynactin (Bennett and Lorenzo, 2016). The function of the DEATH domain is unknown, but the CTD that follows the DEATH domain has autoregulatory functions (Hall and Bennett, 1987; Tsytonok et al., 2015).

The long forms or “giant Ankyrins” are specifically expressed in neurons and are localized to synapses and axons. In axons, Ankyrin and Spectrin are periodically spaced every 190 nm (Otsuka et al., 2002; Pielage et al., 2008; Xu et al., 2013). Giant Ankyrins are so named because they are unusually large proteins; in *C. elegans*, the long form is 6,994 amino acids, whereas

the shorter isoform is 1,867 amino acids. Giant Ankyrins contain the conserved domains found in short isoforms but also include a long insertion at the C terminus lacking recognizable domains. The insertion is encoded in large part by a single exon composed of unconserved DNA repeats in worms, flies, and mice (Jenkins et al., 2015; Koch et al., 2008; Otsuka et al., 2002; Pielage et al., 2008; Stephan et al., 2015).

CK1 δ is required to switch expression from the short isoform to the long isoform of Ankyrin, and the long isoform stabilizes the axon architecture of the nervous system. What is the giant isoform doing that the short isoform cannot? The mechanism is not understood, but where it has been tested, giant ankyrin appears to inhibit axon branching. Specific loss of giant Ankyrin leads to axon defects in *C. elegans* and cultured mouse neurons (Hedgecock et al., 1985; McIntire et al., 1992; Otsuka et al., 1995, 2002; Yang et al., 2019). Giant Ankyrin also plays a role in synapse stability: loss of Ank2-L in *Drosophila* causes the disassembly and retraction of neuromuscular junctions (Koch et al., 2008; Pielage et al., 2008). Giant Ankyrin is also required to maintain the spacing and localization of microtubules in *Drosophila* axons and cultured mouse neurons (Ank2-XL and AnkB, respectively) (Fréal et al., 2016; Stephan et al., 2015; Yang et al., 2019). Which of these represents the primary defect is not known.

Molecular Mechanism of Termination at the Proximal Ankyrin Polyadenylation Site

The giant form of Ankyrin in *C. elegans* is generated when RNA polymerase reads through alternative polyadenylation sites in the *unc-44* locus and incorporates the giant exon into the transcript. In the absence of CK1 δ , transcription is terminated at the proximal polyA site, and giant Ankyrin is not made. The suppressors of *kin-20* prevent termination at the proximal site, and giant Ankyrin is restored. Thus, these mutations tell us what processes are required for termination at alternative polyadenylation sites. In overview, termination is controlled by the phosphorylation pattern of the CTD of RNA polymerase and specific sequence motifs in the nascent mRNA. After the nascent transcript is cut, polyadenylated, and released, the RNA polymerase must release the DNA and terminate transcription. Our genetic analysis suggests a model for how the RNA polymerase machinery directs selection of the proximal alternative polyadenylation site in the *unc-44* gene and how CK1 δ blocks termination in neurons.

The first step in termination is likely to be the dephosphorylation of the CTD of RNA polymerase by the phosphatase SSUP-72. SSUP-72 was previously implicated in stimulating pausing and termination at the *unc-44* polyA site #2 (Chen et al., 2015). SSUP-72 functions by dephosphorylating the CTD of RNA polymerase subunit 1 (RPB1) (Krishnamurthy et al., 2004). The CTD comprises heptad amino acid repeats: 26 in *S. cerevisiae*, 42 in *C. elegans*, and 52 in mammals, encompassing the amino acid sequence YSPTSPS. Phosphorylation of the CTD domain controls the state of the RNA polymerase complex by recruiting

is ≥ 80 . For the wild type and *kin-20(ox423)*, data are repeated from Figure 1. All comparisons were made with Dunnett's multiple comparison test, error bars represent \pm SEM.

(D) Expression of giant ankyrin rescues axon morphology of the CK1 δ mutant. Compared with *kin-20(ox423)*, axon morphology of a *kin-20(ox423)* strain expressing the giant isoform of ankyrin is largely rescued; occasionally, an axon is branched or spindly (EG9248).

elongation or termination factors. Phosphorylation of Ser5 in each repeat signals active transcription and processivity of the polymerase. During termination, the phosphorylation state of the CTD is rewritten. This requires the prolyl-isomerase PINN-1 to reshape the CTD, which allows the phosphatase SSUP-72 to erase the phosphate code (Krishnamurthy et al., 2004; Xiang et al., 2010). Specifically, SSUP-72 de-phosphorylates Serine 5 (Ser5) of the CTD, a key step in the transition from transcription elongation to termination (Kuehner et al., 2011).

In neurons, CK1 δ prevents termination at the proximal polyadenylation site by inhibiting SSUP-72. Ser39 of SSUP-72 is a conserved consensus phosphorylation site for casein kinases (p[S/T]xx[S/T]). Phosphorylation of the first S/T residue primes phosphorylation of the second S/T by CK1 δ (Knippschild et al., 2005). Mutations in SSUP-72 were previously found to restore a subtle loss of giant Ankyrin in *sydn-1* mutant animals, SYDN-1 is a worm-specific nuclear protein thought to promote readthrough during polyA site regulation (Chen et al., 2015). We found that CK1 δ phosphorylates SSUP-72 *in vitro*, and the phosphomimetic mutation S39E bypasses the loss of CK1 δ and restores motility in *kin-20* nulls. Most of the other *kin-20* suppressor alleles that we isolated in SSUP-72 are predicted to eliminate phosphatase activity (Rosado-Lugo and Hampsey, 2014; Xiang et al., 2010).

In the simplest model, CK1 δ phosphorylates Ser39 of SSUP-72, which disrupts phosphatase activity. The phosphorylated CTD of the polymerase maintains the processive state; the polymerase reads through the polyadenylation signal to generate the long form of *unc-44*. CK1 δ is known to bind the CTD of RNA polymerase: the yeast homolog of CK1 δ , Hrr25, directly binds the CTD in a phosphorylation-dependent manner (Phatnani and Greenleaf, 2006). Hrr25 requires Ser2 and Ser5 to be phosphorylated—the state of the CTD during elongation—placing the kinase at the correct transcriptional time and place to phosphorylate SSUP-72.

An alternative but not a mutually exclusive model is that SSUP-72 maintains a gene loop within the Ankyrin gene. Gene loops form when the termination site is associated with the gene's promoter and thereby couples transcription termination to transcription reinitiation. In addition to a role in transcription termination, SSUP-72 is required for gene loop formation (Ansari and Hampsey, 2005; Perkins et al., 2008; Singh and Hampsey, 2007; Tan-Wong et al., 2012). Thus, SSUP-72 may form a gene loop that promotes expression of the short form of Ankyrin. Loss of SSUP-72 function would disrupt loop formation, and the polymerase would proceed through the pause site and transcribe the giant isoform. In fact, Ank2 in mouse neurons forms multiple gene loops both including and excluding the giant exon (Bertolini et al., 2019). CK1 δ phosphorylation of SSUP-72 may constitute the first example of gene loop regulation.

In the absence of CK1 δ , dephosphorylation of Ser5 on the CTD allows for the binding of the Cleavage Factor II complex (CF II). The CF II complex comprises PCF11 and CLP1 (Zhang and Gilmour, 2006; Zhang et al., 2005). PCF11 is recruited to the CTD by Ser2-P, binds the nascent RNA, and disrupts the elongation complex (Licatalosi et al., 2002; Meinhart and Cramer, 2004; Zhang and Gilmour, 2006). The PCF-11(F83Y) mutation we recovered is in the CTD-binding domain (Meinhart and Cramer, 2004) and therefore is likely to interfere with PCF-11 recruitment

to the CTD, thereby leading to an increase in giant Ankyrin mRNA. These results are consistent with an observed increase in transcription readthrough in yeast, flies, and human cells depleted of PCF-11 (Baejen et al., 2017; West and Proudfoot, 2008; Zhang and Gilmour, 2006). Interestingly, PCF-11 is specifically involved in selecting proximal polyA sites in alternative gene isoforms in mammalian cells (Wang et al., 2019).

Selection of a site for cleavage and polyadenylation is under the control of the CPSF complex. There are two nucleotide motifs that coordinate transcription termination and polyadenylation (Figure S4). The canonical polyadenylation site AAUAAA is recognized by CPSF and pauses elongation; the U-rich downstream elements (DSEs) are recognized and bound by the cleavage stimulation factor complex (CstF) (Porrua and Libri, 2015). The transcript is cleaved by CPSF and polyadenylated at a CA dinucleotide 18–30 nucleotides after the AAUAAA motif (Porrua and Libri, 2015). Transcription is terminated no more than 150 nucleotides downstream of the cleavage site, probably coincident and mechanistically linked to cleavage and polyadenylation of the mRNA (Bentley, 2014).

Four of our suppressor mutations are in residues of the CPSF complex (Figure 6), which is responsible for recognizing the AAUAAA polyadenylation signaling motif. One mutation is in PFS-2 in the AAUAAA binding pocket at an interface with CPSF-4 (Clerici et al., 2018); the identical mutation was isolated in a suppression screen of an RNA polymerase subunit in *C. elegans* (Van Epps et al., 2010). Three other mutated residues are on the surface of CPSF-4 directly adjacent to the binding pocket. (Casañal et al., 2017; Clerici et al., 2018). These residues are positioned to potentially convey AAUAAA recognition, directly to the RNA polymerase or possibly via the Paf1 complex.

The Paf1 complex binds and recruits the CPSF complex to the polymerase via multiple interactions (Nordick et al., 2008; Rozenblatt-Rosen et al., 2009). Thus, it is possible that the surface residues that we identified in the CPSF complex are communicating with the RNA polymerase via the Paf1 complex. Specifically, we recovered mutations on surface residues of the CTR-9 protein (Figure 6) (Vos et al., 2018). These mutations are within the main domain composed of 19 pairs of α helices (Vos et al., 2018). We also recovered a mutation in CDC-73, which is the main subunit that recruits the CPSF complex to the polymerase (Nordick et al., 2008; Rozenblatt-Rosen et al., 2009). CDC-73 also links the Paf1 complex to the chromatin of actively transcribed genes (Amrich et al., 2012; Rozenblatt-Rosen et al., 2009). The most abundant target was ZFP-3/ZC3H4 (7 mutations), which has been shown to bind the Paf1 protein and components of the CstF cleavage stimulation complex in high-throughput screens (Li et al., 2004; Stark et al., 2006). ZFP-3 was previously identified in the screens for termination defects in the genes *lin-15* and *unc-44* (Chen et al., 2015; Cui et al., 2008).

The mutations in RNA polymerase recovered in our screen also suggest a role for the Paf1 complex in termination. RPB-2(S101L) disrupts an interaction site with the Paf1C member LEO-1 (Mueller and Jaehning, 2002; Vos et al., 2018). Although direct contacts between LEO-1 and the RPB-2 residues M600 and I603 could not be resolved, electron density from LEO-1 was observed at this position (S. Vos, personal communication). The RPB-2 residues Y537 and V540 are deep within a pocket

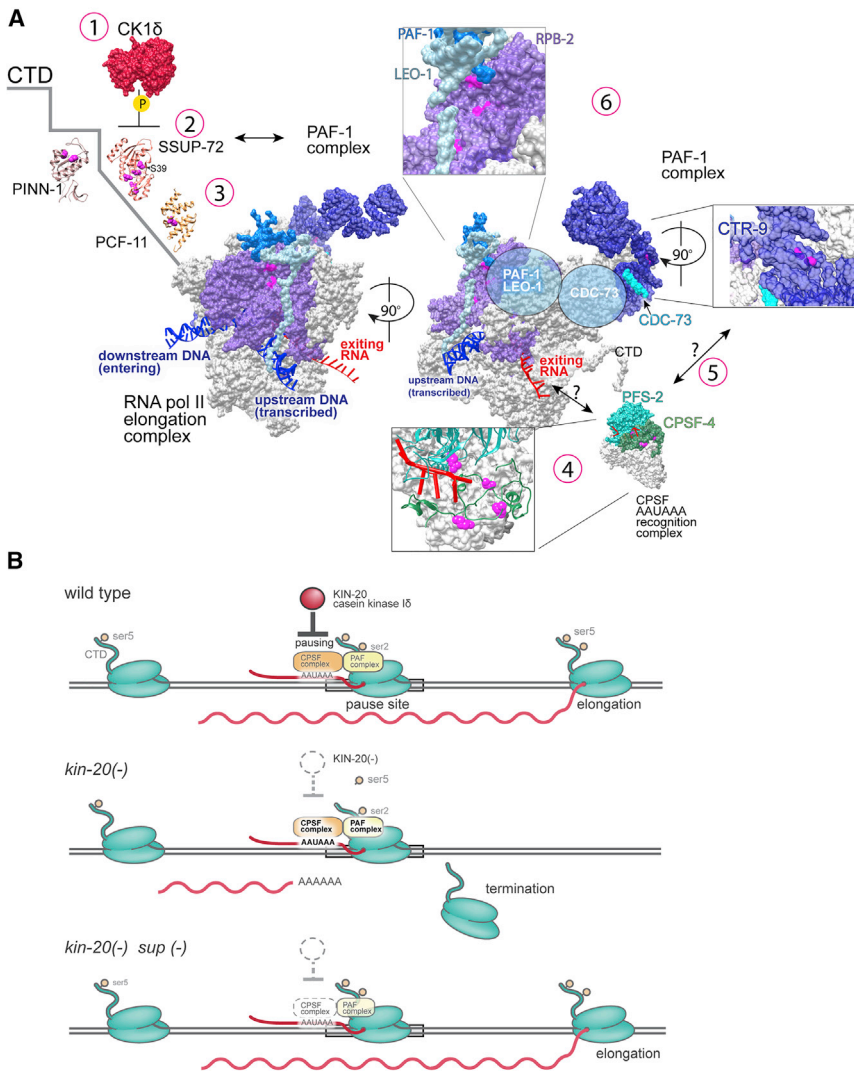


Figure 6. CK1 δ Suppressors Describe a Pathway in Transcription Termination

(A) The *kin-20(ox423)* suppressor screen generated mutations in the RNA polymerase II complex involved in termination (see Table S2 for full list). The genetics and structure together describe a pathway for transcription termination at the *unc-44* second polyadenylation site.

(1) CK1 is associated with the C-terminal domain (CTD) of RNA polymerase subunit RPB-1 (Phatnani and Greenleaf, 2006). In differentiated neurons, CK1 δ phosphorylates SSUP-72 and thereby inhibits remodeling of the CTD. This step is likely the key regulatory step in the switch from expression of short to long ankyrin. (2) The phosphatase SSUP-72 requires the prolyl isomerase PINN-1 to isomerize proline-6 in the heptad repeat so that SSUP-72 can hydrolyze Ser5-P (Werner-Allen et al., 2011; Xu et al., 2003). (3) PCF-11 binds the CTD after dephosphorylation of Ser5-P. PCF-11 interacts with the transcribed RNA and CPSF complex. (4) The CPSF complex recognizes the AAUAAA motif and signals for cleavage and polyadenylation. Mutations in the binding pocket formed by the PFS-2 and CPSF-4 likely interfere with recognition of the polyA signal motif. Mutations of CPSF-4 surface residues may interfere with transduction of that signal. (5) The elongation Paf1 complex is also required for termination at the *unc-44* polyadenylation site. The Paf1 complex recruits CPSF to RNA polymerase and possibly SSUP-72 to the CTD.

(6) Alternatively, the Paf1 complex could be acting as a transduction pathway to the RNA polymerase. Suppressor mutations in the Paf1 complex were obtained in CTR-9, CDC-73, and potential interaction sites in the RPB-2 polymerase subunit.

(B) Model. Top: wild type. When the elongating RNA polymerase II (Pol II) complex approaches PolyA #2, KIN-20/CK1 δ phosphorylates SSUP-72. Phosphorylation inhibits association with the CPSF complex, promoting Pol II processivity. Middle: *kin-20* null. Without CK1 δ , CPSF is recruited to the RNA pol II complex and pauses at the

polyA site. The transcript is cleaved at downstream CA elements terminating transcription at the middle isoform of *unc-44*. Bottom: *kin-20* null and suppressor double mutants, KIN-20/CK1 δ is no longer able to inhibit pausing, resulting in production of *unc-44* long.

that does not interact with LEO-1 directly but may nevertheless destabilize LEO-1 interactions.

The Paf1 complex is normally associated with the initiation and elongation phases of transcription (Jaehning, 2010); however, our genetic data suggest that it is intimately involved in transcription termination in *unc-44*. In addition, mutations in the Paf1 complex in yeast suggest that loss of the complex affects 3' end formation and polyadenylation, again, indicating that the complex also functions during termination (Jaehning, 2010). How the Paf1 complex contributes to termination is not clear. The complex may simply recruit cleavage and polyadenylation factors to the polymerase; our mutations that destabilize the Paf1 complex could lead to a failure to recruit termination machinery. Alternatively, the complex might be involved in transducing cleavage and polyadenylation signals to the RNA polymerase to terminate transcription and dismount from the DNA helix. The mutations we identified may be specifically involved in transducing that allosteric signal.

It is curious that *unc-44* was the only gene exhibiting premature termination in *kin-20* mutants. One might expect that CK1 δ could potentially act on the termination complex of all genes expressed in neurons. It is likely that specificity factors recruit KIN-20 to particular transcription units. For example, the SSUP-72 binding protein SYDN-1 selects among alternative polyadenylation sites in different tissues in the nematode (Chen et al., 2015; Van Epps et al., 2010). SYDN-1 biases transcription toward the long isoform of the *unc-44* gene but the short isoform of the *dlk-1* gene. Thus, SYDN-1 is likely to be a polyadenylation site selector protein rather than a part of the termination complex, whereas KIN-20 apparently only acts as an anti-termination factor on the *unc-44* gene.

Is this mechanism for the generation of giant ankyrin likely to be conserved in other organisms? The ankyrin genes of other invertebrates such as *Drosophila* have ankyrin gene models that are consistent with giant exon selection by alternative polyadenylation sites. Vertebrate ankyrins generate the giant isoform

by alternatively splicing rather than alternative termination (Bennett and Lorenzo, 2016), suggesting that this mechanism of isoform selection is not conserved. On the other hand, it is possible that gene loop formation is the mechanism of isoform selection in both invertebrates and vertebrates. Polyadenylation sites are required for gene loop formation (Perkins et al., 2008), and the alternative exons in vertebrate Ankyrins are preceded and followed by canonical polyadenylation and transcriptional pause sites. It is possible that the machinery for polyadenylation site recognition, such as SSUP-72 and the CPSF complex, may be involved in alternative splicing as well as termination because transcriptional pausing affects splice site availability (Herzel et al., 2017). In fact, splicing itself may drive gene loop formation, a cause and effect conundrum that is being actively investigated (Herzel et al., 2017; Moabbi et al., 2012).

How Does CK1 δ Function as a Maturation Signal?

It is possible that CK1 δ is active in all neurons at their birth to make the axon-specific, long isoform of Ankyrin. However, it is intriguing that axon outgrowth and synapse formation is normal in CK1 δ mutants, that is, a single growth cone maintains apical dominance at the tip of the axon, and synapses are assembled normally on muscles. Only after the axons reach their targets and build synapses do growth cones sprout from the cell body or shaft of mature axons in the CK1 δ mutant. Presumably in the wild type, expression of the long isoform of Ankyrin coincides with synapse formation, and further growth cone initiation is blocked. An intriguing possibility is that the synapse itself launches the signaling cascade. Such a retrograde signal must be upstream of CK1 δ because the kinase is localized and functions in the nucleus. CK1 δ then instructs the nucleus to adopt a mature profile. By contrast, in the CK1 δ mutant, the neuron remains forever young and in a juvenile state.

STAR★METHODS

Detailed methods are provided in the online version of this paper and include the following:

- KEY RESOURCES TABLE
- LEAD CONTACT AND MATERIALS AVAILABILITY
- EXPERIMENTAL MODEL AND SUBJECT DETAILS
 - Strains
 - *kin-20(ox423)* and Wild-Type Axon Quantification
 - *kin-20* Gene Locus
 - Generation of Super-Resolution Tags by CRISPR/Cas9
 - Super-Resolution Imaging
 - Time-Lapse Imaging
 - KIN-20 Localization
 - *kin-20(ox423)* Motor Neuron Confocal Microscopy
 - Tissue-Specific Rescue of *kin-20* Mutants
 - Uncoordinated Screen, Generating the *kin-20(ox423)* Allele
 - *kin-20(ox423)* Suppressor Screen
 - *kin-20* Suppressor Identification
 - Generating Endogenous Point Mutations
 - Axotomy

- Mapping Strains
- qPCR
- *unc-44* Long Overexpression in *kin-20(ox423)*
- *unc-44(ox686)* Molecular Analysis
- RNA Seq
- SSUP-72 Protein Purification
- Radioactive *In Vitro* Kinase Assay
- Protein Structure Visualization
- QUANTIFICATION AND STATISTICAL ANALYSIS
 - KIN-20 Quantification
 - Worm Track Quantification
 - Axons
 - RNA Seq
 - qPCR
- DATA AND CODE AVAILABILITY
 - R-script for Mutation Filtering

SUPPLEMENTAL INFORMATION

Supplemental Information can be found online at <https://doi.org/10.1016/j.devcel.2019.12.005>.

ACKNOWLEDGMENTS

We thank the students of Biol531 Genetics Lab class for isolating the *kin-20(ox423)* mutation: Nels Jorgensen for *kin-20* strain construction; Craig Kaplan for conversations about RNA Pol II structure and termination and connecting us with ideas and people within the field; Seychelle Vos, Lucas Farnung, and Patrick Cramer for sharing unpublished results; Rob Hobson and Nathan Okerlund for assistance imaging EG9581; and Wayne Davis, Matt Schwartz, and Matt Rich for suggestions to improve the manuscript. M.L.L. was supported by a predoctoral training fellowship from the National Institute of Health under award number 5T32GM007464. This work was supported by NINDS R01 NS034307 to (E.M.J.) and NIGMS R35 GM119540 (J.H.). E.M.J. is an investigator of the Howard Hughes Medical Institute.

AUTHOR CONTRIBUTIONS

Conceptualization, M.L.L. and E.M.J.; Methodology, M.L.L., K.A.M., E.J.H., S.A.M., R.L.R., J.H., M.J.B., and E.M.J.; Formal Analysis, M.L.L., K.A.M., E.J.H., and M.J.B.; Investigation, M.L.L., K.A.M., E.J.H., P.D.A., R.L.R., M.A., and M.J.B.; Writing – Original Draft, M.L.L.; Writing – Review and Editing, M.L.L., E.J.H., M.A., M.J.B., and E.M.J.; Visualization, M.L.L.; Project Administration, M.L.L., J.H., M.J.B., and E.M.J.; Funding Acquisition, J.H., M.J.B., and E.M.J.

DECLARATION OF INTERESTS

The authors declare no competing interests.

Received: June 27, 2019
 Revised: October 9, 2019
 Accepted: December 10, 2019
 Published: January 6, 2020

SUPPORTING CITATIONS

The following references appear in the Supplemental Information: Richard and Manley, 2009; Sidorenkov et al., 1998; Xiang et al., 2014.

REFERENCES

- Allen, B.L., and Taatjes, D.J. (2015). The mediator complex: a central integrator of transcription. *Nat. Rev. Mol. Cell Biol.* 16, 155–166.
- Amrich, C.G., Davis, C.P., Rogal, W.P., Shirra, M.K., Heroux, A., Gardner, R.G., Arndt, K.M., and VanDemark, A.P. (2012). Cdc73 subunit of Paf1 complex

- contains C-terminal Ras-like domain that promotes association of Paf1 complex with chromatin. *J. Biol. Chem.* **287**, 10863–10875.
- Anders, S., Reyes, A., and Huber, W. (2012). Detecting differential usage of exons from RNA-seq data. *Genome Res.* **22**, 2008–2017.
- Ansari, A., and Hampsey, M. (2005). A role for the CPF 3'-end processing machinery in RNAP II-dependent gene looping. *Genes Dev.* **19**, 2969–2978.
- Baejen, C., Andreani, J., Torkler, P., Battaglia, S., Schwalb, B., Lidschreiber, M., Maier, K.C., Boltendahl, A., Rus, P., Esslinger, S., et al. (2017). Genome-wide analysis of RNA polymerase II termination at protein-coding genes. *Mol. Cell* **66**, 38–49.e6.
- Banerjee, D., Kwok, A., Lin, S.Y., and Slack, F.J. (2005). Developmental timing in *C. elegans* is regulated by kin-20 and tim-1, homologs of core circadian clock genes. *Dev. Cell* **8**, 287–295.
- Bennett, V., Davis, J., and Fowler, W.E. (1982). Brain spectrin, a membrane-associated protein related in structure and function to erythrocyte spectrin. *Nature* **299**, 126–131.
- Bennett, V., and Lorenzo, D.N. (2013). Spectrin- and ankyrin-based membrane domains and the evolution of vertebrates. *Curr. Top. Membr.* **72**, 1–37.
- Bennett, V., and Lorenzo, D.N. (2016). An adaptable spectrin/ankyrin-based mechanism for long-range organization of plasma membranes in vertebrate tissues. *Curr. Top. Membr.* **77**, 143–184.
- Bentley, D.L. (2014). Coupling mRNA processing with transcription in time and space. *Nat. Rev. Genet.* **15**, 163–175.
- Bertolini, J.A., Favaro, R., Zhu, Y., Pagin, M., Ngan, C.Y., Wong, C.H., Tjong, H., Vermunt, M.W., Martynoga, B., Barone, C., et al. (2019). Mapping the global chromatin connectivity network for Sox2 function in neural stem cell maintenance. *Cell Stem Cell* **24**, 462–476.e6.
- Brenner, S. (1974). The genetics of *Caenorhabditis elegans*. *Genetics* **77**, 71–94.
- Byrne, A.B., Walratt, T., Gardner, K.E., Hubbert, A., Reinke, V., and Hammarlund, M. (2014). Insulin/IGF1 signaling inhibits age-dependent axon regeneration. *Neuron* **81**, 561–573.
- C. elegans* Deletion Mutant Consortium (2012). Large-scale screening for targeted knockouts in the *Caenorhabditis elegans* genome. *G3 (Bethesda)* **11**, 1415–1425.
- Casañal, A., Kumar, A., Hill, C.H., Easter, A.D., Emsley, P., Degliesposti, G., Gordiyenko, Y., Santhanam, B., Wolf, J., Wiederhold, K., et al. (2017). Architecture of eukaryotic mRNA 3'-end processing machinery. *Science* **358**, 1056–1059.
- Chen, F., Chisholm, A.D., and Jin, Y. (2017). Tissue-specific regulation of alternative polyadenylation represses expression of a neuronal ankyrin isoform in *C. elegans* epidermal development. *Development* **144**, 698–707.
- Chen, F., Zhou, Y., Qi, Y.B., Khivansara, V., Li, H., Chun, S.Y., Kim, J.K., Fu, X.D., and Jin, Y. (2015). Context-dependent modulation of Pol II CTD phosphatase SSUP-72 regulates alternative polyadenylation in neuronal development. *Genes Dev.* **29**, 2377–2390.
- Clerici, M., Faini, M., Muckenfuss, L.M., Aebersold, R., and Jinek, M. (2018). Structural basis of AAUAAA polyadenylation signal recognition by the human CPSF complex. *Nat. Struct. Mol. Biol.* **25**, 135–138.
- Cui, M., Allen, M.A., Larsen, A., Macmorris, M., Han, M., and Blumenthal, T. (2008). Genes involved in pre-mRNA 3'-end formation and transcription termination revealed by a lin-15 operon Muv suppressor screen. *Proc. Natl. Acad. Sci. USA* **105**, 16665–16670.
- Dobin, A., Davis, C.A., Schlesinger, F., Drenkow, J., Zaleski, C., Jha, S., Batut, P., Chaisson, M., and Gingeras, T.R. (2013). STAR: ultrafast universal RNA-seq aligner. *Bioinformatics* **29**, 15–21.
- Essers, P.B., Nonnekens, J., Goos, Y.J., Betist, M.C., Viester, M.D., Mossink, B., Lansu, N., Korswagen, H.C., Jelier, R., Brenkman, A.B., et al. (2015). A long noncoding RNA on the ribosome is required for lifespan extension. *Cell Rep.* **10**, 339–345.
- Fish, K.J., Cegielska, A., Getman, M.E., Landes, G.M., and Virshup, D.M. (1995). Isolation and characterization of human casein kinase I ϵ (CKI), a novel member of the CKI gene family. *J. Biol. Chem.* **270**, 14875–14883.
- Fréal, A., Fassier, C., Le Bras, B., Bullier, E., De Gois, S., Hazan, J., Hoogenraad, C.C., and Couraud, F. (2016). Cooperative interactions between 480 kDa ankyrin-G and EB proteins assemble the axon initial segment. *J. Neurosci.* **36**, 4421–4433.
- Frøkjær-Jensen, C., Davis, M.W., Ailion, M., and Jorgensen, E.M. (2012). Improved Mos1-mediated transgenesis in *C. elegans*. *Nat. Methods* **9**, 117–118.
- Frøkjær-Jensen, C., Davis, M.W., Hopkins, C.E., Newman, B.J., Thummel, J.M., Olesen, S.P., Grunnet, M., and Jorgensen, E.M. (2008). Single-copy insertion of transgenes in *Caenorhabditis elegans*. *Nat. Genet.* **40**, 1375–1383.
- Frøkjær-Jensen, C., Davis, M.W., Sarov, M., Taylor, J., Filibotte, S., LaBella, M., Pozniakovsky, A., Moerman, D.G., and Jorgensen, E.M. (2014). Random and targeted transgene insertion in *Caenorhabditis elegans* using a modified Mos1 transposon. *Nat. Methods* **11**, 529–534.
- Gabel, C.V., Antoine, F., Chuang, C.F., Samuel, A.D.T., and Chang, C. (2008). Distinct cellular and molecular mechanisms mediate initial axon development and adult-stage axon regeneration in *C. elegans*. *Development* **135**, 1129–1136.
- Gross, S., and Moore, C. (2001). Five subunits are required for reconstitution of the cleavage and polyadenylation activities of *Saccharomyces cerevisiae* cleavage factor I. *Proc. Natl. Acad. Sci. USA* **98**, 6080–6085.
- Hall, T.G., and Bennett, V. (1987). Regulatory domains of erythrocyte ankyrin. *J. Biol. Chem.* **262**, 10537–10545.
- Hallam, S.J., and Jin, Y. (1998). lin-14 regulates the timing of synaptic remodeling in *Caenorhabditis elegans*. *Nature* **395**, 78–82.
- Hammarlund, M., Davis, W.S., and Jorgensen, E.M. (2000). Mutations in beta-spectrin disrupt axon outgrowth and sarcomere structure. *J. Cell Biol.* **149**, 931–942.
- Hammarlund, M., Jorgensen, E.M., and Bastiani, M.J. (2007). Axons break in animals lacking beta-spectrin. *J. Cell Biol.* **176**, 269–275.
- Hammarlund, M., Nix, P., Hauth, L., Jorgensen, E.M., and Bastiani, M. (2009). Axon regeneration requires a conserved MAP kinase pathway. *Science* **323**, 802–806.
- Hedgecock, E.M., Culotti, J.G., Thomson, J.N., and Perkins, L.A. (1985). Axonal guidance mutants of *Caenorhabditis elegans* identified by filling sensory neurons with fluorescein dyes. *Dev. Biol.* **111**, 158–170.
- Herzel, L., Ottoz, D.S.M., Alpert, T., and Neugebauer, K.M. (2017). Splicing and transcription touch base: co-transcriptional spliceosome assembly and function. *Nat. Rev. Mol. Cell Biol.* **18**, 637–650.
- Hobert, O. (2002). PCR fusion-based approach to create reporter gene constructs for expression analysis in transgenic *C. elegans*. *Biotechniques* **32**, 728–730.
- Hollopeter, G., Lange, J.J., Zhang, Y., Vu, T.N., Gu, M., Ailion, M., Lambie, E.J., Slaughter, B.D., Unruh, J.R., Florens, L., et al. (2014). The membrane-associated proteins FCHO and SGIP are allosteric activators of the AP2 clathrin adaptor complex. *eLife* **3**.
- Hsin, J.P., and Manley, J.L. (2012). The RNA polymerase II CTD coordinates transcription and RNA processing. *Genes Dev.* **26**, 2119–2137.
- Jaehning, J.A. (2010). The Paf1 complex: platform or player in RNA polymerase II transcription? *Biochim. Biophys. Acta* **1799**, 379–388.
- Jegla, T., Nguyen, M.M., Feng, C., Goetschius, D.J., Luna, E., van Rossum, D.B., Kamel, B., Pisupati, A., Milner, E.S., and Rolls, M.M. (2016). Bilateral giant ankyrins have a common evolutionary origin and play a conserved role in patterning the axon initial segment. *PLoS Genet.* **12**, e1006457.
- Jenkins, P.M., Kim, N., Jones, S.L., Tseng, W.C., Svitkina, T.M., Yin, H.H., and Bennett, V. (2015). Giant ankyrin-G: a critical innovation in vertebrate evolution of fast and integrated neuronal signaling. *Proc. Natl. Acad. Sci. USA* **112**, 957–964.
- Juette, M.F., Gould, T.J., Lessard, M.D., Mlodzianoski, M.J., Nagpure, B.S., Bennett, B.T., Hess, S.T., and Bewersdorf, J. (2008). Three-dimensional sub-100 nm resolution fluorescence microscopy of thick samples. *Nat. Methods* **5**, 527–529.

- Kloss, B., Price, J.L., Saez, L., Blau, J., Rothenfluh, A., Wesley, C.S., and Young, M.W. (1998). The *Drosophila* clock gene *double-time* encodes a protein closely related to human casein kinase I ϵ . *Cell* **94**, 97–107.
- Knippschild, U., Gocht, A., Wolff, S., Huber, N., Löhler, J., and Stöter, M. (2005). The casein kinase 1 family: participation in multiple cellular processes in eukaryotes. *Cell. Signal.* **17**, 675–689.
- Knobel, K.M., Davis, W.S., Jorgensen, E.M., and Bastiani, M.J. (2001). UNC-119 suppresses axon branching in *C. elegans*. *Development* **128**, 4079–4092.
- Knobel, K.M., Jorgensen, E.M., and Bastiani, M.J. (1999). Growth cones stall and collapse during axon outgrowth in *Caenorhabditis elegans*. *Development* **126**, 4489–4498.
- Koch, I., Schwarz, H., Beuchle, D., Goellner, B., Langeegger, M., and Aberle, H. (2008). *Drosophila* ankyrin 2 is required for synaptic stability. *Neuron* **58**, 210–222.
- Koenig, S.N., and Mohler, P.J. (2017). The evolving role of ankyrin-B in cardiovascular disease. *Heart Rhythm* **14**, 1884–1889.
- Kordeli, E., Lambert, S., and Bennett, V. (1995). AnkyrinG. A new ankyrin gene with neural-specific isoforms localized at the axonal initial segment and node of Ranvier. *J. Biol. Chem.* **270**, 2352–2359.
- Krishnamurthy, S., He, X., Reyes-Reyes, M., Moore, C., and Hampsey, M. (2004). Ssu72 is an RNA polymerase II CTD phosphatase. *Mol. Cell* **14**, 387–394.
- Kuehner, J.N., Pearson, E.L., and Moore, C. (2011). Unravelling the means to an end: RNA polymerase II transcription termination. *Nat. Rev. Mol. Cell Biol.* **12**, 283–294.
- Kunimoto, M., Otto, E., and Bennett, V. (1991). A new 440-kD isoform is the major ankyrin in neonatal rat brain. *J. Cell Biol.* **115**, 1319–1331.
- Kurshan, P.T., Merrill, S.A., Dong, Y., Ding, C., Hammarlund, M., Bai, J., Jorgensen, E.M., and Shen, K. (2018). γ -Neurexin and frizzled mediate parallel synapse assembly pathways antagonized by receptor endocytosis. *Neuron* **100**, 150–166.e4.
- Kurup, N., and Jin, Y. (2015). Neural circuit rewiring: insights from DD synapse remodeling. *Worm* **5**, e1129486.
- Li, P., Merrill, S.A., Jorgensen, E.M., and Shen, K. (2016). Two clathrin adaptor protein complexes instruct axon-dendrite polarity. *Neuron* **90**, 564–580.
- Li, S., Armstrong, C.M., Bertin, N., Ge, H., Milstein, S., Boxem, M., Vidalain, P.O., Han, J.D., Chesneau, A., Hao, T., et al. (2004). A map of the interactome network of the metazoan *C. elegans*. *Science* **303**, 540–543.
- Licatalosi, D.D., Geiger, G., Minet, M., Schroeder, S., Cilli, K., McNeil, J.B., and Bentley, D.L. (2002). Functional interaction of yeast pre-mRNA 3' end processing factors with RNA polymerase II. *Mol. Cell* **9**, 1101–1111.
- Love, M.I., Huber, W., and Anders, S. (2014). Moderated estimation of fold change and dispersion for RNA-seq data with DESeq2. *Genome Biol.* **15**, 550.
- McIntire, S.L., Garriga, G., White, J., Jacobson, D., and Horvitz, H.R. (1992). Genes necessary for directed axonal elongation or fasciculation in *C. elegans*. *Neuron* **8**, 307–322.
- Meinhart, A., and Cramer, P. (2004). Recognition of RNA polymerase II carboxy-terminal domain by 3'-RNA-processing factors. *Nature* **430**, 223–226.
- Minevich, G., Park, D.S., Blankenberg, D., Poole, R.J., and Hobert, O. (2012). CloudMap: a cloud-based pipeline for analysis of mutant genome sequences. *Genetics* **192**, 1249–1269.
- Mlodzianoski, M.J., Juette, M.F., Beane, G.L., and Bewersdorf, J. (2009). Experimental characterization of 3D localization techniques for particle tracking and super-resolution microscopy. *Opt. Express* **17**, 8264–8277.
- Moabbi, A.M., Agarwal, N., El Kaderi, B.E., and Ansari, A. (2012). Role for gene looping in intron-mediated enhancement of transcription. *Proc. Natl. Acad. Sci. USA* **109**, 8505–8510.
- Mueller, C.L., and Jaehning, J.A. (2002). Ctr9, Rtf1, and Leo1 are components of the Paf1/RNA polymerase II complex. *Mol. Cell Biol.* **22**, 1971–1980.
- Nix, P., Hisamoto, N., Matsumoto, K., and Bastiani, M. (2011). Axon regeneration requires coordinate activation of p38 and JNK MAPK pathways. *Proc. Natl. Acad. Sci. USA* **108**, 10738–10743.
- Nordick, K., Hoffman, M.G., Betz, J.L., and Jaehning, J.A. (2008). Direct interactions between the Paf1 complex and a cleavage and polyadenylation factor are revealed by dissociation of Paf1 from RNA polymerase II. *Eukaryot. Cell* **7**, 1158–1167.
- Otsuka, A.J., Boontrakulpoontawee, P., Rebeiz, N., Domanus, M., Otsuka, D., Velampampil, N., Chan, S., Vande Wyngaerde, M., Campagna, S., and Cox, A. (2002). Novel UNC-44 AO13 ankyrin is required for axonal guidance in *C. elegans*, contains six highly repetitive STEP blocks separated by seven potential transmembrane domains, and is localized to neuronal processes and the periphery of neural cell bodies. *J. Neurobiol.* **50**, 333–349.
- Otsuka, A.J., Franco, R., Yang, B., Shim, K.H., Tang, L.Z., Zhang, Y.Y., Boontrakulpoontawee, P., Jeyaprakash, A., Hedgecock, E., and Wheaton, V.I. (1995). An ankyrin-related gene (*unc-44*) is necessary for proper axonal guidance in *Caenorhabditis elegans*. *J. Cell Biol.* **129**, 1081–1092.
- Perkins, K.J., Lusic, M., Mitar, I., Giacca, M., and Proudfoot, N.J. (2008). Transcription-dependent gene looping of the HIV-1 provirus is dictated by recognition of pre-mRNA processing signals. *Mol. Cell* **29**, 56–68.
- Petersen, E.F., Goddard, T.D., Huang, C.C., Couch, G.S., Greenblatt, D.M., Meng, E.C., and Ferrin, T.E. (2004). UCSF Chimera—a visualization system for exploratory research and analysis. *J. Comput. Chem.* **25**, 1605–1612.
- Phatnani, H.P., and Greenleaf, A.L. (2006). Phosphorylation and functions of the RNA polymerase II CTD. *Genes Dev.* **20**, 2922–2936.
- Pielage, J., Cheng, L., Fetter, R.D., Carlton, P.M., Sedat, J.W., and Davis, G.W. (2008). A presynaptic giant ankyrin stabilizes the NMJ through regulation of presynaptic microtubules and transsynaptic cell adhesion. *Neuron* **58**, 195–209.
- Pokala, N., Liu, Q., Gordus, A., and Bargmann, C.I. (2014). Inducible and titratable silencing of *Caenorhabditis elegans* neurons in vivo with histamine-gated chloride channels. *Proc. Natl. Acad. Sci. USA* **111**, 2770–2775.
- Porrua, O., and Libri, D. (2015). Transcription termination and the control of the transcriptome: why, where and how to stop. *Nat. Rev. Mol. Cell Biol.* **16**, 190–202.
- Price, J.L., Blau, J., Rothenfluh, A., Abodeely, M., Kloss, B., and Young, M.W. (1998). *double-time* is a novel *Drosophila* clock gene that regulates PERIOD protein accumulation. *Cell* **94**, 83–95.
- Rhodehouse, K., Cascino, K., Aseltine, L., Padula, A., Weinstein, R., Spina, J.S., Olivero, C.E., and Van Wynsberghe, P.M. (2018). The doubletime homolog *KIN-20* mainly regulates *let-7* independently of its effects on the period homolog *LIN-42* in *Caenorhabditis elegans*. *G3 (Bethesda)* **8**, 2617–2629.
- Richard, P., and Manley, J.L. (2009). Transcription termination by nuclear RNA polymerases. *Genes Dev.* **23**, 1247–1269.
- Rosado-Lugo, J.D., and Hampsey, M. (2014). The Ssu72 phosphatase mediates the RNA polymerase II initiation-elongation transition. *J. Biol. Chem.* **289**, 33916–33926.
- Rozenblatt-Rosen, O., Nagaïke, T., Francis, J.M., Kaneko, S., Glatt, K.A., Hughes, C.M., LaFramboise, T., Manley, J.L., and Meyerson, M. (2009). The tumor suppressor Cdc73 functionally associates with CPSF and CstF 3' mRNA processing factors. *Proc. Natl. Acad. Sci. USA* **106**, 755–760.
- Schwartz, M.L., and Jorgensen, E.M. (2016). SapTrap, a toolkit for high-throughput CRISPR/Cas9 gene modification in *Caenorhabditis elegans*. *Genetics* **202**, 1277–1288.
- Shilatifard, A. (2012). The COMPASS family of histone H3K4 methylases: mechanisms of regulation in development and disease pathogenesis. *Annu. Rev. Biochem.* **81**, 65–95.
- Shinohara, Y., Koyama, Y.M., Ukai-Tadenuma, M., Hirokawa, T., Kikuchi, M., Yamada, R.G., Ukai, H., Fujishima, H., Umehara, T., Tainaka, K., and Ueda, H.R. (2017). Temperature-sensitive substrate and product binding underlie temperature-compensated phosphorylation in the clock. *Mol. Cell* **67**, 783–798.e20.
- Sidorenkov, I., Komissarova, N., and Kashlev, M. (1998). Crucial role of the RNA: DNA hybrid in the processivity of transcription. *Mol. Cell* **2**, 55–64.
- Singh, B.N., and Hampsey, M. (2007). A transcription-independent role for TFIIB in gene looping. *Mol. Cell* **27**, 806–816.

- Stark, C., Breikreutz, B.J., Reguly, T., Boucher, L., Breikreutz, A., and Tyers, M. (2006). BioGRID: a general repository for interaction datasets. *Nucleic Acids Res.* *34*, D535–D539.
- Stephan, R., Goellner, B., Moreno, E., Frank, C.A., Hugenschmidt, T., Genoud, C., Aberle, H., and Pielage, J. (2015). Hierarchical microtubule organization controls axon caliber and transport and determines synaptic structure and stability. *Dev. Cell* *33*, 5–21.
- Stiernagle, T. (2006). Maintenance of *C. elegans* (WormBook).
- Sulston, J.E. (1976). Post-embryonic development in the ventral cord of *Caenorhabditis elegans*. *Philos. Trans. R. Soc. Lond. B Biol. Sci.* *275*, 287–297.
- Tan-Wong, S.M., Zaugg, J.B., Camblong, J., Xu, Z., Zhang, D.W., Mischo, H.E., Ansari, A.Z., Luscombe, N.M., Steinmetz, L.M., and Proudfoot, N.J. (2012). Gene loops enhance transcriptional directionality. *Science* *338*, 671–675.
- Temmerman, L., Meelkop, E., Janssen, T., Bogaerts, A., Lindemans, M., Husson, S.J., Beets, I., and Schoofs, L. (2011). *C. elegans* homologs of insect clock proteins: a tale of many stories. *Ann. N. Y. Acad. Sci.* *1220*, 137–148.
- Tennessen, J.M., Gardner, H.F., Volk, M.L., and Rougvie, A.E. (2006). Novel heterochronic functions of the *Caenorhabditis elegans* period-related protein LIN-42. *Dev. Biol.* *289*, 30–43.
- Tennessen, J.M., Opperman, K.J., and Rougvie, A.E. (2010). The *C. elegans* developmental timing protein LIN-42 regulates diapause in response to environmental cues. *Development* *137*, 3501–3511.
- Tsytlonok, M., Ibrahim, S.M., Rowling, P.J.E., Xu, W., Ruedas-Rama, M.J., Orte, A., Klenerman, D., and Itzhaki, L.S. (2015). Single-molecule FRET reveals hidden complexity in a protein energy landscape. *Structure* *23*, 190–198.
- Van Epps, H., Dai, Y., Qi, Y., Goncharov, A., and Jin, Y. (2010). Nuclear pre-mRNA 3'-end processing regulates synapse and axon development in *C. elegans*. *Development* *137*, 2237–2250.
- Verdecia, M.A., Bowman, M.E., Lu, K.P., Hunter, T., and Noel, J.P. (2000). Structural basis for phosphoserine-proline recognition by group IV WW domains. *Nat. Struct. Biol.* *7*, 639–643.
- Vos, S.M., Farnung, L., Boehning, M., Wigge, C., Linden, A., Urlaub, H., and Cramer, P. (2018). Structure of activated transcription complex Pol II–DSIF–PAF–SPT6. *Nature* *560*, 607–612.
- Wang, R., Zheng, D., Wei, L., Ding, Q., and Tian, B. (2019). Regulation of intronic polyadenylation by PCF11 impacts mRNA expression of long genes. *Cell Rep* *26*, 2766–2778.e6.
- Werner-Allen, J.W., Lee, C.J., Liu, P., Nicely, N.I., Wang, S., Greenleaf, A.L., and Zhou, P. (2011). cis-Proline-mediated Ser(P)5 dephosphorylation by the RNA polymerase II C-terminal domain phosphatase Ssu72. *J. Biol. Chem.* *286*, 5717–5726.
- West, S., and Proudfoot, N.J. (2008). Human Pcf11 enhances degradation of RNA polymerase II-associated nascent RNA and transcriptional termination. *Nucleic Acids Res.* *36*, 905–914.
- White, J.G., Albertson, D.G., and Anness, M.A. (1978). Connectivity changes in a class of motoneuron during the development of a nematode. *Nature* *271*, 764–766.
- White, J.G., Southgate, E., Thomson, J.N., and Brenner, S. (1986). The structure of the nervous system of the nematode *Caenorhabditis elegans*. *Philos. Trans. R. Soc. Lond. B Biol. Sci.* *314*, 1–340.
- Wu, Z., Ghosh-Roy, A., Yanik, M.F., Zhang, J.Z., Jin, Y., and Chisholm, A.D. (2007). *Caenorhabditis elegans* neuronal regeneration is influenced by life stage, ephrin signaling, and synaptic branching. *Proc. Natl. Acad. Sci. USA* *104*, 15132–15137.
- Xiang, K., Nagaïke, T., Xiang, S., Kilic, T., Beh, M.M., Manley, J.L., and Tong, L. (2010). Crystal structure of the human symplekin-Ssu72-CTD phosphopeptide complex. *Nature* *467*, 729–733.
- Xiang, K., Tong, L., and Manley, J.L. (2014). Delineating the structural blueprint of the pre-mRNA 3'-end processing machinery. *Mol. Cell. Biol.* *34*, 1894–1910.
- Xu, K., Zhong, G., and Zhuang, X. (2013). Actin, spectrin, and associated proteins form a periodic cytoskeletal structure in axons. *Science* *339*, 452–456.
- Xu, Y.X., Hirose, Y., Zhou, X.Z., Lu, K.P., and Manley, J.L. (2003). Pin1 modulates the structure and function of human RNA polymerase II. *Genes Dev.* *17*, 2765–2776.
- Yang, R., Walder-Christensen, K.K., Kim, N., Wu, D., Lorenzo, D.N., Badea, A., Jiang, Y.H., Yin, H.H., Wetsel, W.C., and Bennett, V. (2019). ANK2 autism mutation targeting giant ankyrin-B promotes axon branching and ectopic connectivity. *Proc. Natl. Acad. Sci. USA* *116*, 15262–15271.
- Young, M.W., and Kay, S.A. (2001). Time zones: a comparative genetics of circadian clocks. *Nat. Rev. Genet.* *2*, 702–715.
- Zhang, H., Constantine, R., Vorobiev, S., Chen, Y., Seetharaman, J., Huang, Y.J., Xiao, R., Montelione, G.T., Gerstner, C.D., Davis, M.W., et al. (2011). UNC119 is required for G protein trafficking in sensory neurons. *Nat. Neurosci.* *14*, 874–880.
- Zhang, X., Chen, X., Zeng, Z., Zhang, M., Sun, Y., Xi, P., Peng, J., and Xu, P. (2015). Development of a reversibly switchable fluorescent protein for super-resolution optical fluctuation imaging (SOFI). *ACS Nano* *9*, 2659–2667.
- Zhang, Z., Fu, J., and Gilmour, D.S. (2005). CTD-dependent dismantling of the RNA polymerase II elongation complex by the pre-mRNA 3'-end processing factor, Pcf11. *Genes Dev.* *19*, 1572–1580.
- Zhang, Z., and Gilmour, D.S. (2006). Pcf11 is a termination factor in *Drosophila* that dismantles the elongation complex by bridging the CTD of RNA polymerase II to the nascent transcript. *Mol. Cell* *21*, 65–74.
- Zou, Y., Chiu, H., Zinovyeva, A., Ambros, V., Chuang, C.F., and Chang, C. (2013). Developmental decline in neuronal regeneration by the progressive change of two intrinsic timers. *Science* *340*, 372–376.

STAR★METHODS

KEY RESOURCES TABLE

REAGENT or RESOURCE	SOURCE	IDENTIFIER
Bacterial and Virus Strains		
BL21	Lab stock	N/A
TOP 10	Lab stock	N/A
Chemicals, Peptides, and Recombinant Proteins		
CK1 delta	NEB	P6030
Software and Algorithms		
SNP filtering	This paper: https://github.com/jorgensenlab/WGS-variant-filtering	N/A
GraphPad prism	https://www.graphpad.com/scientific-software/prism/	N/A
STAR aligner	https://github.com/alexdobin/STAR	N/A
DESeq2	https://bioconductor.org/packages/release/bioc/html/DESeq2.html	N/A
DEXseq	https://bioconductor.org/packages/release/bioc/html/DEXSeq.html	N/A
Burrows-Wheeler Aligner	http://bio-bwa.sourceforge.net/	N/A
Unified genotyper GATK	https://software.broadinstitute.org/gatk/documentation/tooldocs/3.8-0/org_broadinstitute_gatk_tools_walkers_genotyper_UnifiedGenotyper.php	N/A
SNPEff	http://snpeff.sourceforge.net/	N/A
ApE A plasmid Editor	https://jorgensen.biology.utah.edu/wayned/ape/	N/A
Fiji – Fiji is just imageJ	https://fiji.sc/	N/A
SapTrap builder	https://www.micropublication.org/journals/biology/m4qq-2x02/	N/A
Primer3Plus	http://www.bioinformatics.nl/cgi-bin/primer3plus/primer3plus.cgi	N/A
WormLab	https://www.mbfioscience.com/wormlab	N/A
Vutara SRX	https://www.bruker.com/products/fluorescence-microscopes/vutara-super-resolution-microscopy/overview/srx-software-vutara-super-resolution.html	N/A
Zeiss LSM5 Pascal	No longer supported	N/A
Zeiss LSM510	No longer supported	N/A
Zeiss ZEN black	https://www.zeiss.com/microscopy/us/products/microscope-software/zen-lite.html	N/A
Nikon I series	https://www.nikon.com/products/microscope-solutions/support/download/software/biological/90i_v24432.htm	N/A

LEAD CONTACT AND MATERIALS AVAILABILITY

Further information and requests for resources and reagents should be directed to and will be fulfilled by the Lead Contact, Erik M. Jorgensen Jorgensen@biology.utah.edu.

EXPERIMENTAL MODEL AND SUBJECT DETAILS

Strains

C. elegans strains were grown and maintained using standard methods (Brenner, 1974). The wild type is N2 Bristol. For a full list of strains and mutations used in this work, see [Key Resources Table](#).

kin-20(ox423) and Wild-Type Axon Quantification

C. elegans hermaphrodites were immobilized for microscopy on a 2% agarose pad in M9 + 25mM sodium azide solution on a glass slide. Animals were allowed to equilibrate for 5 minutes. The cover slip was sealed with Vaseline. Animals were imaged on a Zeiss LSM 510 META with a 60X oil immersion lens (Carl Zeiss, Jena, Germany). Right side was imaged because GABA motor neurons in the ventral cord send commissures along the right side of the body wall to the dorsal nerve cord. Spectral unmixing was performed to remove auto-fluorescence in gut granules, allowing better visualization of the motor neuron commissures to be scored.

kin-20 Gene Locus

Six isoforms are generated by alternative splicing of 5' and 3' exons. The large 5' exon is only found in the genus *Caenorhabditis*. All isoforms contain a conserved casein kinase 1 domain. The *ok505* allele is a complete deletion of the kinase domain and an out-of-frame insertion. KIN-20 was fluorescently tagged at the start of the second exon, after the alternative start-site methionine, with tagRFP (*oxSi1087*). The second exon is the start of the conserved kinase domain found in all isoforms. Inserting the fluorophore at this exon tags all isoforms.

Generation of Super-Resolution Tags by CRISPR/Cas9

nrx-1, *rimb-1*, and *syd-2* were endogenously tagged by CRISPR-mediated insertion of DNA encoding SkyLAN-s using the SapTrap toolkit as previously described (Schwartz and Jorgensen, 2016). A single plasmid containing the repair template and guide RNA was built using the SapTrap plasmid assembly. The repair template was composed of 57bp homology arms and SKYLAN-S (Zhang et al., 2015) containing a *loxP::unc-119(+):loxP*. The SapTrap assembled plasmid was mixed with plasmids to express Cas9 in the germline, a histamine-gated chloride channel in neurons (Pokala et al., 2014), and fluorescent array markers. This mix was injected into the gonads of young adult EG9823 animals. After selecting for *unc-119(+)* and selecting against extrachromosomal arrays by histamine application, and loss of the fluorescent array markers, animals were injected with pDD104[*Peft-3::CRE*], selected for excision of *loxP::unc-119::loxP*, and 1x outcrossed before super-resolution microscopy.

Super-Resolution Imaging

Methods are similar to those described (Kurshan et al., 2018; Li et al., 2016). 3D super-resolution images were recorded with a Vutara SR 350 biplane microscope (Bruker, Nanosurfaces, Inc., Madison, WI) (Juetten et al., 2008; Mlodzianoski et al., 2009). Live intact *C. elegans* L2 larva were immobilized for microscopy on a 2% agarose pad in M9 + 50mM sodium azide solution on a glass slide and the cover slip was sealed with Vaseline. The ventral cord in the region of the developing germline was positioned directly against the cover slip and imaged to avoid the intestinal auto-fluorescent granules. SKYLAN-S was excited by 488nm light at 1kW/cm² and photoactivated by 405nm light. Images were recorded using a 60x/1.2 NA Olympus water immersion objective and Hamamatsu Flash4 V1 sCMOS camera with the gain set at 50 and frame rate at 50 Hz. Vutara SRX software (version 6.02) was used in data analysis. The background was removed, and single molecule localizations were identified based on brightness in each frame. Three dimensional localizations were obtained by fitting the raw data in a 12x12-pixel region of interest centered around each particle in each plane with a 3D model function built from recorded bead data sets. A density-based denoising algorithm to remove isolated particles was used for filtering. The remaining localizations were classified into clusters by density-based spatial clustering of applications with noise (DBSCAN), and a minimum of 10 localizations were connected around a 100nm search radius.

Time-Lapse Imaging

Methods are similar to those described (Knobel et al., 1999) with the following changes. Worms were immobilized for microscopy by placing them on a mixture of 1ul of 2.65% polystyrene 0.1um diameter beads in water and 1ul 20mM muscimol on an agarose pad under a cover slip. Slides were sealed with Vaseline to prevent evaporation. Time-lapse images were collected (Nikon Eclipse 90i) every 3 minutes over a Z range of 10-15 μm at 0.1 μm/pixel resolution. Figure 2A VD growth cones in a wild-type larva expressing GFP in GABA neurons (EG1285), Figure 2B VD growth cones in a *kin-20(ox423)* early L2 larva, Figure 2C L1 larva, Figure 2D *kin-20(ox423)* L1 larva.

KIN-20 Localization

Preparation of worms for microscopy was done as previously described above. Animals for Figures S3B and S3C were imaged on an Opterra swept-field confocal microscope (Bruker) using a 60x 1.2NA water objective. Images were captured on an EM-CCD camera (Hamamatsu ImagemX2). Animals for Figures 3F, 3G, and S3D–S3H were imaged on the Zeiss LSM 880 confocal microscope using a 63x oil objective.

kin-20(ox423) Motor Neuron Confocal Microscopy

Preparation of worms for microscopy was done as previously described. Animals were imaged on the Pascal LSM5 (Zeiss) with a 63x 1.4NA oil objective. Z-stacks were acquired through the entire animal then a Z-projection from maximum intensity was made using ImageJ. Z-projections were stitched together with the MosaicJ plugin in ImageJ. The *oxIs12* allele was used for expressing soluble GFP in GABA neurons.

Tissue-Specific Rescue of *kin-20* Mutants

kin-20(ox423) animals expressing soluble GFP in GABA neurons were injected with a *kin-20* cDNA rescue gene under different promoters expressing in different tissues as seen in (construct details in Table S1). Minigenes were assembled with Gateway cloning. *kin-20* cDNA was amplified from *C. elegans* cDNA library constructed from Superscript-III kits from Invitrogen. The *kin-20* cDNA was amplified based on isoform 'B', which is simply the kinase domain and a small exon C-terminally. This isoform excludes the alternate first exon as seen in Figure 1F. The *let-858* 3'UTR was used for each construct.

kin-20 null animals have a low frequency of transgenic array formation for an unknown reason. The only constructs that were able to form stable transgenic arrays were those that could also rescue the null phenotype, ubiquitous expression, and pan-neuronal expression. This result suggests that array formation in *kin-20* nulls is so low, a rescue construct is necessary to stabilize the array. Note, germline expression from an array is highly unlikely. The two constructs designed to express in the gametes would need to be integrated to assess rescue potential. This approach was abandoned since the genetics of the *kin-20* maternal effect rescue indicated that germline contribution of KIN-20 gene products are sufficient to rescue offspring neuron defects in *kin-20* mutant animals.

Uncoordination Screen, Generating the *kin-20(ox423)* Allele

The *kin-20(ox423)* premature stop allele was generated in a screen looking for uncoordinated mutants. Adult hermaphrodites were mutagenized using 50mM ethyl methanesulfonate (EMS) (Brenner, 1974), and 3,544 haploid genomes were screened for constipated phenotypes. These were then rescreened in the F3 for behavioral defects. *ox423* was dumpy and paralyzed. Outcrossing demonstrated that *ox423* mutation is maternal effect uncoordinated (Mau); F2 exhibited a constipated phenotype, whereas F3 animals were paralyzed and egg-laying defective. The *kin-20(ox423)* allele failed to complement a *kin-20(ok505)* full deletion allele. The *kin-20(ox423)* mutation was mapped to the X chromosome, then whole-genome sequenced and SNPs were identified to determine the molecular identity. A *kin-20* rescue construct was built using the *kin-20* promoter, gene isoform 'a' and the native 3'UTR, tagging the first common exon with tagRFP (Figure 1F). This construct was inserted as a single copy gene insertion using the MosSCI (Frøkjær-Jensen et al., 2008; Frøkjær-Jensen et al., 2012), and fully rescued *kin-20(ox423)* phenotypes.

kin-20(ox423) Suppressor Screen

Methods are similar to those described (Hollopeter et al., 2014). Late L4 *Caenorhabditis elegans* larvae were mutagenized with 0.5 mM *N*-ethyl-*N*-nitrosourea (ENU) for 4hrs at 22C. Animals were washed with M9 buffer, then ~1000 L4 to young adults were pipetted onto a dense lawn of NA22 *E. coli* grown on 10-cm nematode growth medium (NGM) enriched peptone agar plates, on 66 plates in all. Animals were grown to starvation, then a ~2.5 x 2.5 cm piece of agar was cut from each plate and transferred to new NA22 bacteria on NGM enriched agar plates. In this screen, multiple independent mutagenized populations were generated, each containing enough genetic diversity to give rise to at least one suppressor. The populations were propagated for ~ ten generations, and then one mobile animal was selected from each population.

kin-20 Suppressor Identification

To identify the *kin-20* suppressor mutations, we performed whole-genome resequencing. We first resequenced five suppressor strains to test our method of SNP identification. We did phenotypic mapping experiments with multicolor mapping strains, in which expression constructs were arrayed on different chromosomes (Frøkjær-Jensen et al., 2014). In the first mapping experiment, we found the causative SNP mapped to chromosome II in strain EG8338. There was only a mutation in one conserved gene in our list of candidates on chromosome II in this strain, SSUP-72 S39F, and cloned the mutant gene. We then overexpressed the mutant version of *ssup-72* in a *kin-20* null mutant and were able to rescue the neuronal defect in these animals (data not shown). We Sanger sequenced the remaining suppressor strains at the *ssup-72* locus and found four additional alleles.

We leveraged the known binding partners of SSUP-72 as a candidate gene list and discovered mutations in RPB-2 and PINN-1 among our 5 whole-genome sequenced strains. We discovered four additional alleles of *rpb-2* and three additional alleles of *pinn-1* in our suppressor collection using Sanger sequencing.

To identify the remaining suppressor alleles, 31 strains were resequenced with an average depth of 22-fold. Four components of the RNA polymerase (RNAP) II complex and *unc-44* were identified as suppressors by *in silico* complementation testing, we found multiple alleles in each gene: *zfp-3*, *cpsf-4*, *ctr-9*, and *unc-44* (Minevich et al., 2012). Single mutations in the following suppressors were identified from the sequencing data for their known interactions with the RNAP II complex; *cdc-73*, *pfs-2*, *pcf-11*, and *cdk-8*.

Generating Endogenous Point Mutations

Methods are similar to those described using the SapTrap toolkit (Schwartz and Jorgensen, 2016). One critical update is the use of the EG9881 strain. This strain constitutively expresses *Peft-3::Cas9* and *Phsp::Cre* from an endogenous insertion in chromosome III, as well as a fluorescent maker for easy tracking of the allele. SapTrapv31k software was used to design the potential suppressor point mutations in *pfs-2*, *nrd-1*, *pcf-11*, *cdk-8*, *cdc-73*, and *ssup-72*. Plasmids pMLS415 and pMLS256, as well as the 57 bp homology arm and sgRNA annealed oligos, were annealed into a single plasmid that was injected into the EG9881 strain along with the three array markers (*Prab-3::mCherry::unc-54* UTR, *Pmyo-2::mCherry::unc-54* UTR, *Pmyo-3::mCherry::unc-54* UTR) used in MosSCI (Frøkjær-Jensen et al., 2012). Animals were selected for *unc-119(-)* rescue and no array marker expression. Strains were genotyped by PCR, then heat-shocked to express Cre and selected for *unc-119(+)* loss. Each CRISPR-generated allele was then Sanger sequenced and outcrossed.

Axotomy

Animals were mounted and axotomized as previously described (Hammarlund et al., 2009). Scoring *kin-20* mutants for regeneration after axotomy was more difficult than wild type due to the severity of the branching phenotype. Images were taken immediately after axotomy and then again 24 hours later. These were compared to aid in scoring. If the original axotomized axon was unable to be identified, due to extensive branching, this was still included in the total axons cut and likely underestimated the extent of regeneration. 95% confidence intervals were calculated using the modified Wald method and P values were calculated using the Fisher exact test as previously described (Hammarlund et al., 2009).

Mapping Strains

Fluorescent balancer strains, generated by random gene insertion using miniMos, were crossed together to generate two mapping strains (Frøkjær-Jensen et al., 2014). EG8040 is used to map chromosomes I, II, and III. EG8041 is used to map chromosomes IV, V, and X. These strains also contain a null allele of *him-8* and *him-5* respectively, to spontaneously generate males for crossing. The overexpression of *Peft-3::H2B::GFP* and *Peft-3::H2B::tdTomato* in these strains seems to make the males a bit temperature sensitive. Therefore, the first mapping crosses were done between 15-20°C.

qPCR

C. elegans hermaphrodites were grown on NA22 *E. coli* to adulthood and were dissolved in hypochlorite solution. Embryos were washed, and total RNA was extracted using a Qiagen RNeasy mini kit + Qiagen on-column DNase treatment. Total RNA was then reverse transcribed to cDNA using an Invitrogen Superscript III First-Strand Synthesis System using the supplied oligo(dT) option and using 300ng of total RNA as template. Relative mRNA quantity was measured by qPCR on the Masterplex ep realplex instrument (Eppendorf, Hauppauge, NY) with SYBR green fluorescent dye. cDNA libraries were tested for contaminated gDNA by measuring a reverse transcriptase (-) control.

unc-44 Long Overexpression in *kin-20(ox423)*

kin-20(ox423) mutant animals were injected with overlapping PCR products of the entire *unc-44* gene locus. The PCR products span from the beginning of the 5'UTR to the end of the 3'UTR of the native *unc-44f* locus. However cDNA was used as a template for the region that spanned the polyA site #2, thus amplifying only the long form of *unc-44*. *C. elegans* can assemble a functional gene in an extrachromosomal array by recombination of the overlapping PCR fragments (Hobert, 2002).

unc-44(ox686) Molecular Analysis

The mutation in *unc-44(ox686)* is a three-nucleotide substitution, conserved in nematodes, in the intron preceding exon 15 and the alternative polyA site #2 (Figures 5A and S6B). We synthesized a cDNA library (as previously described) from the *unc-44(ox686)* strain and sequenced from flanking exons across exon 15 using primers oML520 and oML596 (Key Resources Table). We found that exon 15 is skipped in this suppressor and bypasses polyA site #2 resulting in only the long form of Ankyrin. We see no obvious phenotype in these animals which no longer have short form #2 of Ankyrin. However, the short and long isoforms determined by polyA site #1 and #3 are still present in this strain (Figures S6A and 5B).

RNA Seq

C. elegans embryos were prepared using standard methods (Stiernagle, 2006). Three biological replicates were used for each genome. Total RNA was extracted using a Qiagen RNeasy kit. The University of Utah sequencing core did library prep by poly(A) capture and Illumina RNA sequencing.

SSUP-72 Protein Purification

C. elegans ssup-72 and *kin-20* cDNAs were amplified from a *C. elegans* cDNA library with primers oML929/oML930 and oML933/oML934 respectively (Key Resources Table). PCR products were gel purified and cloned by Gibson assembly into the pGEX-6P1 bacterial expression vector and transformed into BL21 chemically competent expression *E. coli*. This vector fuses the GST purification tag to the cloned sequence in the ORF via a PreScission protease linker sequence. A test expression was performed and SSUP-72 and KIN-20 protein were expressed at the correct size (KIN-20 37kDa + GST 26kDa = ~63kDa; SSUP-72 22.8kDa + GST 26kDa = ~49kDa). Samples were run on a 10% polyacrylamide gel and stained with Coomassie G-250 (data not shown).

SSUP-72 was purified in a similar manner to other GST fusion RNA pol II complex components (Gross and Moore, 2001). Starter cultures were first grown O/N in LB with carbenicillin selection. 500ml of terrific broth + carb was inoculated to an OD 0.1 nm and cells were grown at 37°C in baffled flasks shaken at 180rpms to an optical density of 0.5-0.6nm at 37°C. Protein expression was then induced with 0.4mM IPTG and cells were allowed to express for 24hrs at 20°C. Cells were harvested, spun at 7K for 10min at 4°C, washed with wash buffer (1xPBS, 1mM DTT, 1mM EDTA) and bacterial pellets were frozen at -80°C. All purification steps were done at 4°C. Cells were thawed in lysis buffer (50mM Tris/pH7.5, 250mM KCl/1mM EDTA/0.5mM DTT/10% glycerol/1mg/ml lysozyme/Roche protein inhibitor cocktail) and sonicated on a Branson sonicator until lysates clarified slightly and cells were disrupted. Cells debris was removed by centrifugation at 11,000 x g for 30min. The supernatant was diluted with 1:2 volumes of buffer D (20mM Tris HCl, pH8.0/50mM KCl/0.2mM EDTA/ 0.5mM DTT/ 10% Glycerol/Roche protease inhibitor cocktail) and bound to 1ml of glutathione sepharose 4B resin (that had been equilibrated to buffer D) O/N at 4°C on a nutator (GE Cat#17075601). The beads were

washed 4x 15ml PBS and GST was cleaved from the fusion protein using PreScission protease in cleavage buffer (50mM Tris-HCL pH7.5/15mM NaCl/1mM EDTA/1mM DTT/0.01% Triton) as per the GE protocol. Cleaved purified protein was collected through a column, dialyzed to buffer D, and stored at -80C.

KIN-20 was unfortunately insoluble and even after thorough testing of 10 different buffers and many purification conditions the protein remained insoluble in the pellet (data not shown). Since *C. elegans* CK1 δ proved to be insoluble in our hands and because casein kinases are conserved, we purchased recombinant rat CK1 δ protein from NEB (Cat# P06030). This protein is truncated, removing its self-phosphorylated inhibitory domain. Casein kinases self-inhibit so we used the truncated protein as opposed to the full-length purified protein, which has orders of magnitude lower activity (NEB CK1 \sim 1000pmol/min/ul, Abcam purified full-length CK1 δ \sim 8pmol/min/ul).

Radioactive *In Vitro* Kinase Assay

The reaction conditions for the *in vitro* kinase assay were based on the NEB protocol available online. 5ul of purified SSUP-72 substrate was incubated with 2ul of 100ng/ul CK1 δ in NEB protein kinase buffer (50mM Tris-HCl pH7.5/10mM MgCl₂/0.1mM EDTA/2mM DTT/0.01% Brij 35 + 200uM ATP + [γ -32P]ATP) in a reaction volume of 25ul at 30C for 2 hours. The commercially available protein Casein was used as a positive control. Samples (+/- CK1) and controls were run on a Bio-Rad pre-cast gel, washed with 7% acetic acid for 20min, then dried on Whatman 3.0 paper, exposed to a phosphor plate for 1 hour and imaged on a GE-Typhoon.

Protein Structure Visualization

Structure references for the human CPSF complex (cleavage-polyadenylation specificity factor), *S. cerevisiae* PCF-11, murine CK1 δ , human PIN-1, human RNA polymerase II, and human SSUP-72 respectively: (Clerici et al., 2018; Meinhart and Cramer, 2004; Shinohara et al., 2017; Verdecia et al., 2000; Vos et al., 2018; Xiang et al., 2010).

Molecular graphics and analyses performed with UCSF Chimera (Pettersen et al., 2004), developed by the Resource for Bio-computing, Visualization, and Informatics at the University of California, San Francisco, with support from NIH P41-GM103311.

QUANTIFICATION AND STATISTICAL ANALYSIS

KIN-20 Quantification

Quantification of KIN-20 expression for Figure 3C was performed using an optical section at the center of the neuron cell body. The region of interest comprising the cell body was selected using ImageJ software. The fluorescence was measured and normalized to area in ImageJ. Cell bodies were excluded from analysis if the proper cell assignment, either DD or VD, could not be determined, or if an auto-fluorescent gut granule obstructed the image.

Worm Track Quantification

A single *C. elegans* young adult hermaphrodite was placed on a 5cm NGM plate seeded with OP50. The animal behaved freely for 2 minutes, and a photo was taken of the worm track with an Allied Vision Technologies model Stingray camera, using a Nikon AF Micro Nikkor 60mm lens, a MicroBrightField biosciences LED Illuminator, and Micro Bright Field biosciences WormLab (4.1.0) software. Worm tracks were then traced on a WAACOM touchscreen monitor, x,y coordinates and length measurements were taken with in-house ImageJ macros. ImageJ x,y coordinates were transformed into a scalable vector graphics file (svg) with an in-house Tcl script.

Axons

Axon defect counts data were graphed in GraphPad Prism software and analyzed by Welch's unpaired t-tests in GraphPad in Figure 1. Dunnett's multiple comparison test was used for data in Figure 5C.

RNA Seq

Reads were aligned with STAR (Dobin et al., 2013). DEXseq analysis was used for the discovery of mRNA differential expression at the isoform level (Anders et al., 2012). DESeq2 analysis was used for mRNA differential expression at the whole gene level (Love et al., 2014).

Data analysis and graphing was done on GraphPad Prism software.

qPCR

Samples were measured in triplicate, and quantified using a standard curve of pooled, serially diluted samples. Three biological replicates were measured per sample. mRNA quantity was normalized to the quantity of ribosomal protein 18 (*rpl-18*) mRNA. *rpl-18* was selected for its consistent expression level across biological replicates as well as developmental stages, making it an ideal normalization control. *rpl-19*, *eif-3.d*, *ebg-1*, and *clp-3* were also tested by qPCR as potential normalization controls, but in our hands, *rpl-18* was best. Primer design for qPCR reactions was done using Primer3Plus online software. All comparisons were done by Dunnett's multiple comparison test.

DATA AND CODE AVAILABILITY

R-script for Mutation Filtering

The programming language R was used to write a SNP filter with the option to exclude mutations that fall under the following categories: parental, synonymous, intergenic, heterozygous, intronic, and pseudogenes. An *in-silico* complementation test was also written in R. Scripts can be accessed at <https://github.com/jorgensenlab/WGS-variant-filtering>.

Developmental Cell, Volume 52

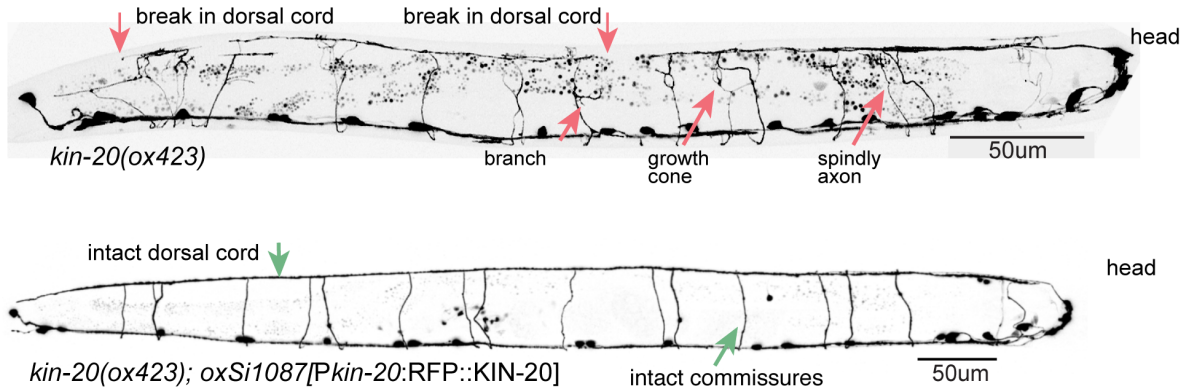
Supplemental Information

**Casein Kinase 1 δ Stabilizes Mature Axons
by Inhibiting Transcription Termination of Ankyrin**

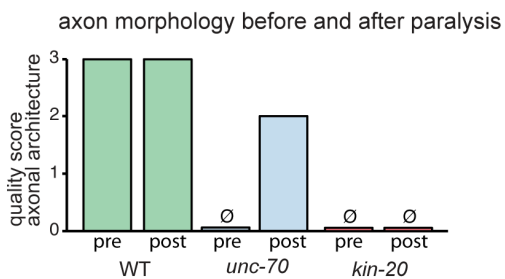
Matthew L. LaBella, Edward J. Hujber, Kristin A. Moore, Randi L. Rawson, Sean A. Merrill, Patrick D. Allaire, Michael Ailion, Julie Hollien, Michael J. Bastiani, and Erik M. Jorgensen

SUPPLEMENTAL INFORMATION

A single-copy KIN-20::RFP rescues *kin-20(-)*



B spontaneous growth in *kin-20(-)*



C active growth cones in *kin-20(-)* after axotomy

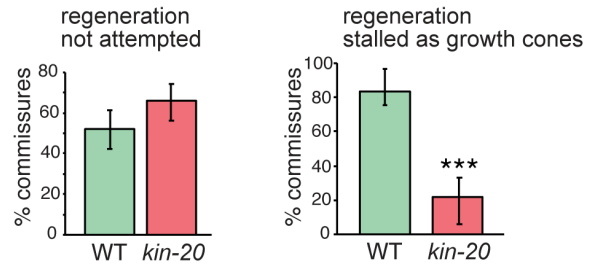


Figure S1. Rescue of *kin-20(ox423)* axon branching defects related to Figures 1 & 2.

(A) Rescue of *kin-20(ox423)* axon branching defects. Above, the *kin-20* mutant displaying maintenance defects marked by red arrows. GFP is soluble and expressed in GABA neurons; images are of L4 animals. Below, *kin-20(ox423)* rescued by a single-copy tagRFP::KIN-20 transgene (*oxSi1087*), including all exons and 8.1kb upstream of the first start site (strain EG9581). Data are quantified in Figure 5C.

(B) CK1δ mutant branching is spontaneous, not break-induced (left). Inhibiting movement of animals by Titin-related / *unc-22* RNAi knockdown rescues axonal branching defects in beta-spectrin / *unc-70(s1502)* mutants (strain EG4980), but not in *kin-20(ox423)* (strain EG5202).

The axon quality score used for analysis was '3' for wild-type in appearance with no defects, '2'

for animals that are mostly wild type with fewer than 5 defects, '1' for animals with moderate axonal defects between 5 -10 per animal, and '0' for animals with major defects, more than 10 per animal, $N \geq 15$.

(C) Most axons in the wild type and *kin-20* mutants do not regenerate after axotomy (middle). GABA commissures were cut by laser axotomy in wild-type and *kin-20(ox423)* animals at L4 stage, then analyzed for regeneration 24 hours later as adults. Left, in both the wild type and *kin-20(ox423)*, most axons do not attempt regeneration; they remain as a stump or retract after axotomy (WT 52%; *kin-20(ox423)* 66%, Fisher exact test $p=0.05$, $n>100$). Bars show the percent of axons that failed to attempt regeneration and a 95% confidence interval (CI). Right, most growth cones stall in cut axons of the wild type (right). Of the axons that attempt regeneration 24 hours after axotomy, 83% of wild-type axons sprout growth cones but fail to grow toward the dorsal cord and are still found at the cut site. By contrast, cut axons that attempt to regenerate in *kin-20* mutants, stall at the cut site only 22% of the time (Fisher exact test $***p=0.0004$, error bars indicate 95% CI, $n>100$). This is consistent with Figure 2G showing that most *kin-20* mutant axons successfully regenerate once the attempt is made.

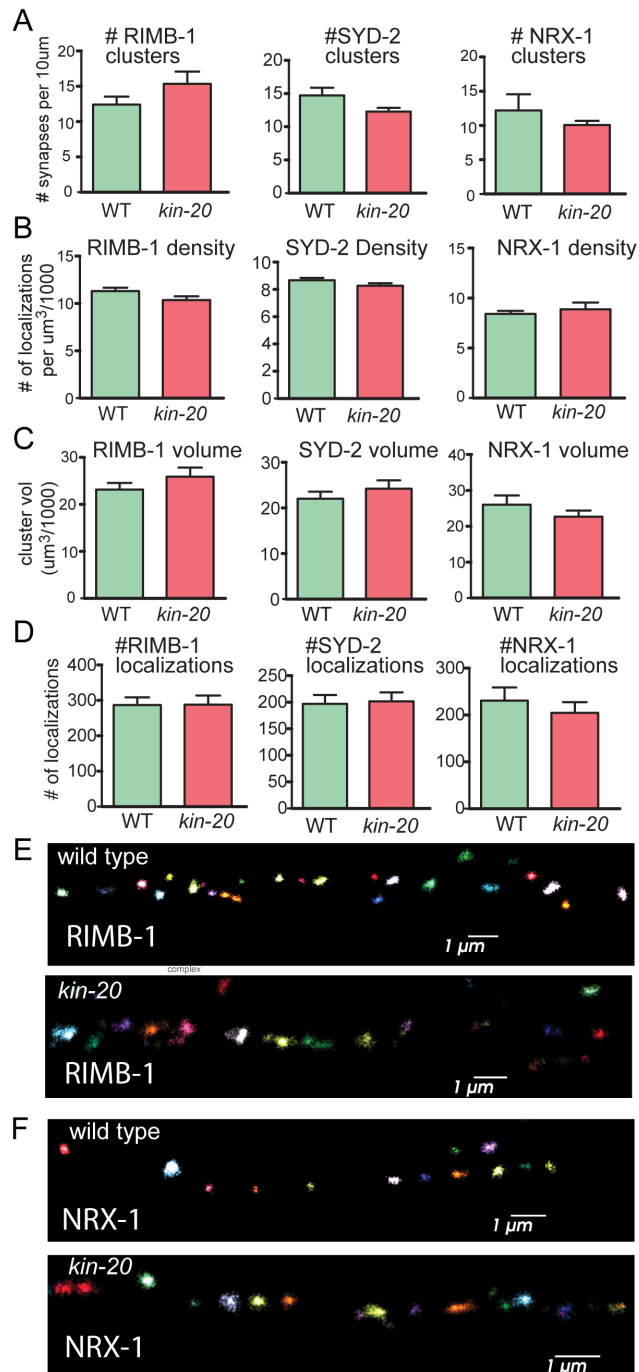


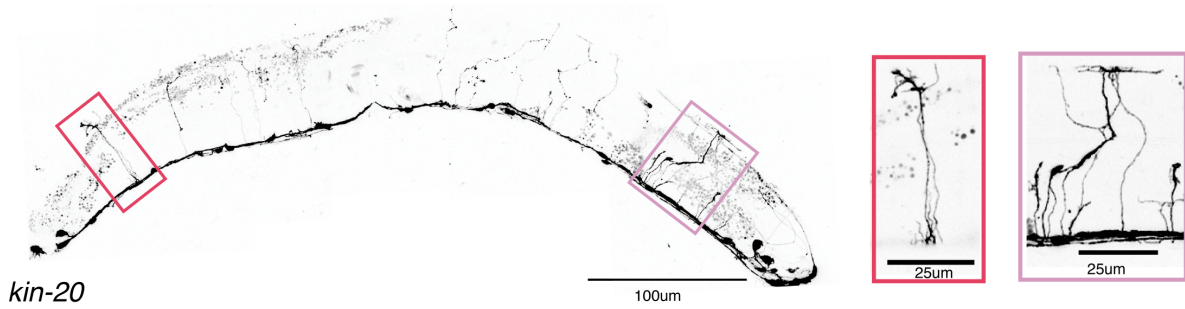
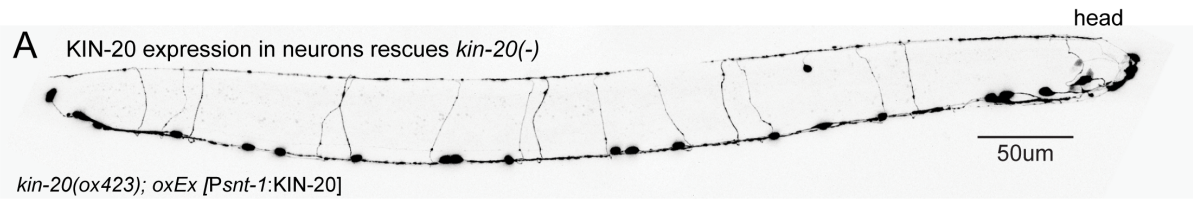
Figure S2. CK1δ is not required for synapse development related to Figure 3.

(A-F) Super-resolution imaging was performed on proteins associated with the presynaptic dense projection: RIMB-1 (RIM-binding protein (Rab3-interacting-binding protein)) (*ox704*), liprin- α / SYD-2 (*ox715*), and neurexin / NRX-1 (*ox719*). Imaging was done on the ventral cord of L2 larval stage animals while VD synapses were forming (Kurup and Jin, 2015). Synapse formation is normal in *kin-20* mutants.

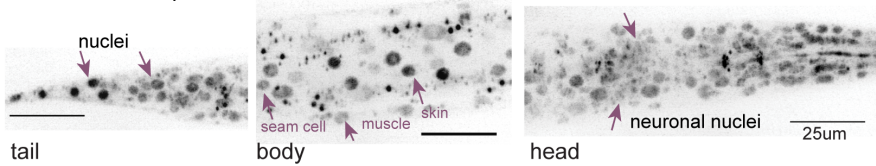
(A-D) Synapses of the wild type and *kin-20* mutants were indistinguishable in all metrics tested. The density, volume, number of synapses (clusters) per length of axon, and the number of synaptic protein localizations were the same comparing wild-type animals and *kin-20(ox423)* mutants. (Data plotted is mean \pm SEM, see STAR methods for full statistics table, strains EG9802-9804).

(E) Synaptic clusters of CRISPR-tagged RIMB-1::Skylan-S are similar in the wild type (EG9802) and *kin-20(ox423)* (EG9803).

(F) Synaptic clusters of CRISPR-tagged NRX-1::Skylan-S are similar in the wild type (EG9785) and *kin-20(ox423)* (EG9786).



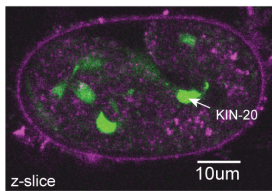
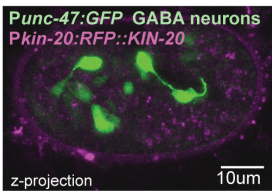
B KIN-20 ubiquitous nuclear localization *kin-20(ox423); oxS[Pkin-20:RFP::KIN-20]*



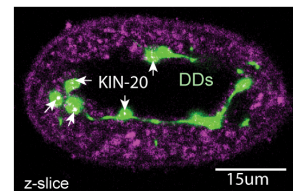
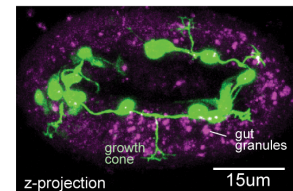
C adherens junctions



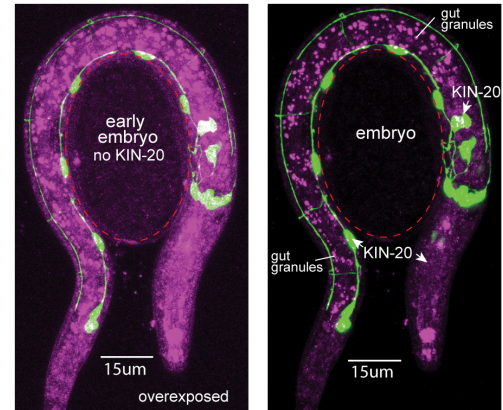
D 1.5-fold embryo



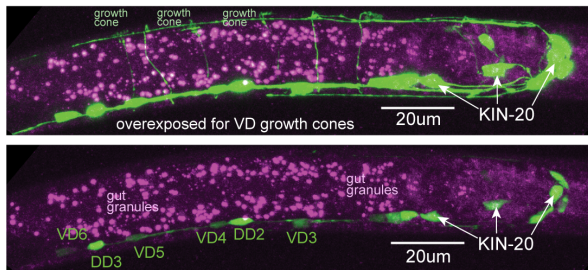
E 3-fold embryo



F early embryo and L1 hatching



G late L1 larva



H L2 larva, KIN-20 nuclear expression

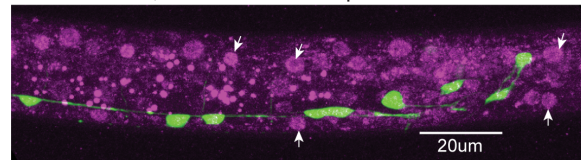


Figure S3. CK1δ functions cell autonomously in neurons and localizes to cell bodies related to Figure 3.

(A) *kin-20(ox423)* mutant nervous system defects are rescued by overexpression of *kin-20* cDNA in neurons under the control of the *snt-1* promoter (strain EG9313).

(B-H) KIN-20 protein localization using a single-copy insertion of a tagged rescuing construct (*oxSi1087[Pkin-20:tagRFP::KIN-20]*) in *kin-20(ox423)* background (Strain EG9581); GABA neurons marked with soluble GFP (*oxIs12*).

(B) CK1δ is ubiquitous and localized to nuclei in L4 larvae. Expression is observed in the epidermis, muscle, seam cells, intestine, and neurons in larval stage animals but not adults (not shown).

(C) KIN-20 is localized at adherens junctions in the spermatheca in the L4.

(D) 1.5-fold embryo. Top, Z-stack of the entire embryo. Below, single confocal slice. Very dim KIN-20 expression is observed in two of the DD neuron cell bodies; KIN-20 expression is otherwise not present in GABA neurons.

(E) 3-fold embryo. Top, Z-stack. The DD neurons have extended along the ventral nerve cord and growth cones are extending toward the dorsal nerve cord. Bottom, single confocal section of DD cell bodies. KIN-20 expression is now visible at this stage in the DD cell bodies.

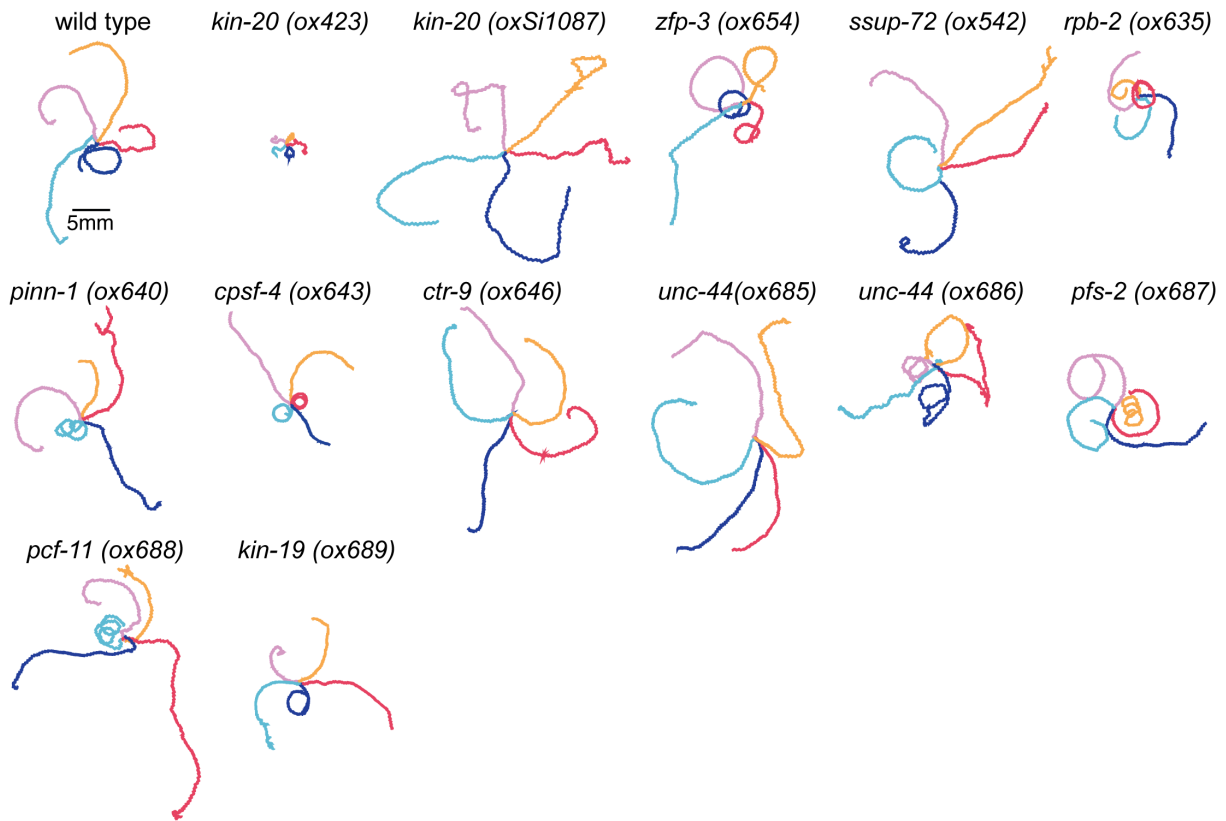
(F) Left, early embryo (outlined with red dots). There is no detectable KIN-20 expression in early embryos preceding morphogenesis. The panel on the left is greatly overexposed to show the outline of the embryo and how dim it is compared to the hatchling. Right, in a newly hatched L1 larva, KIN-20 expression can be clearly seen in DD neuron cell bodies.

(G) During the late L1 to L2 larval stages VD GABA neurons extend axons from the ventral to dorsal surface. The top image is overexposed in the green channel to show the dim axonal commissures and growth cones. KIN-20 expression is clearly visible in the cell bodies of the RMEs, AVL, RIS neurons in the head ganglia, as well as the DD cell bodies along the ventral

cord. The bottom panel shows the dim but visible KIN-20 expression that is increasing in the body of the animal. Bright puncta in the intestine are autofluorescent gut granules. However, KIN-20 expression in VD cell bodies is barely detectable above the background (quantified in Figure 3C).

(H) At the L2 larval stage KIN-20 expression is brightly expressed in non-neuronal nuclei of the epidermis, muscle, and intestine. KIN-20 expression in VD cell bodies is now equal to that in DD cell bodies (quantified in Figure 3C).

A worm tracks *kin-20(ox423)* suppressor double mutants



B SSUP-72 Ssu72p alignment

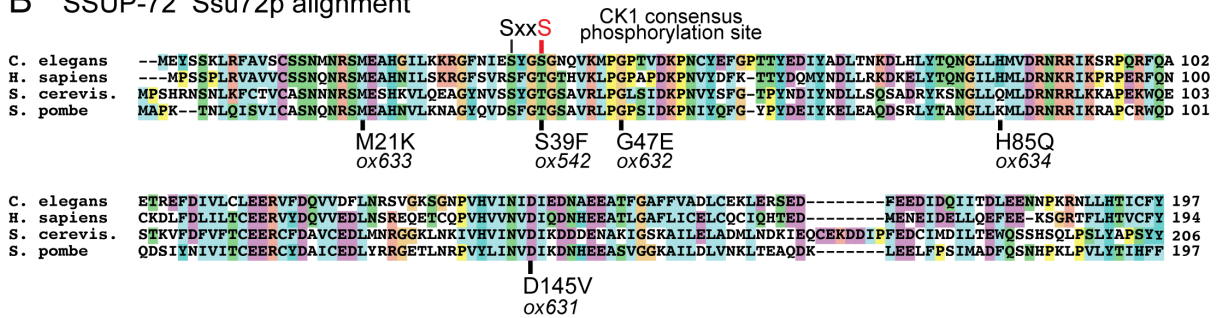
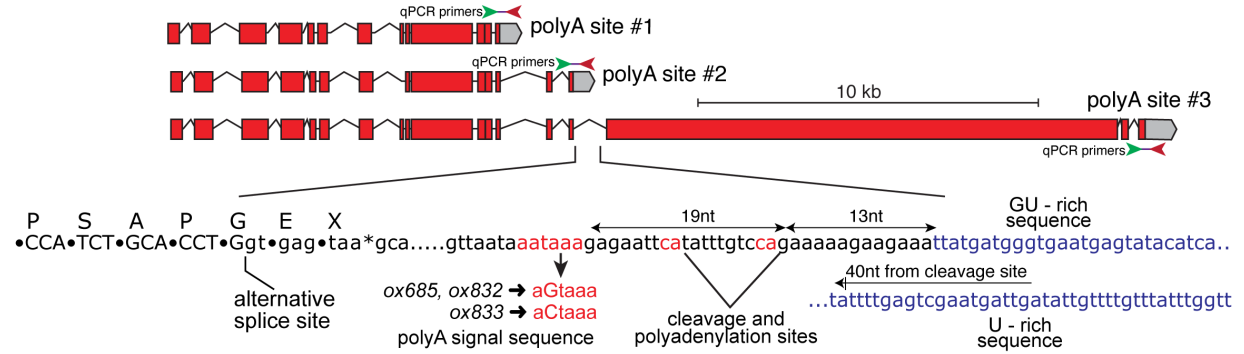


Figure S4. *kin-20(-)* mutants are suppressed by defects in transcription termination related to Figures 4.

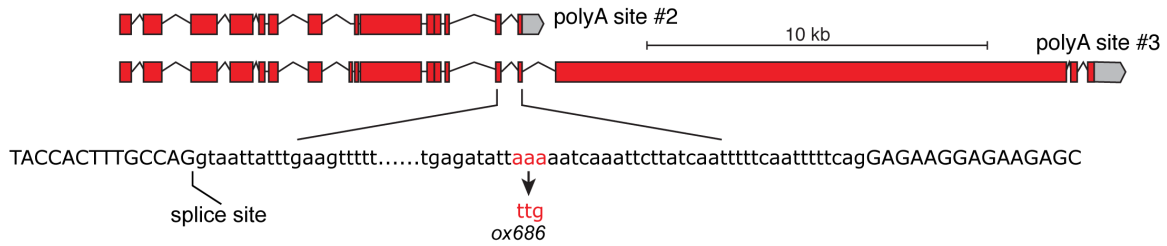
(A) Suppressors restore locomotion to *kin-20(ox423)* mutants. All genotypes are double mutants with *kin-20(ox423)*. Worm tracks recorded for 2 minutes. Each color represents a different animal.

(B) Protein alignment of SSUP-72. The red line indicates the site of the S39F suppressor and the S39E and S39A CRISPR mutations, within the canonical CK1 phosphorylation site. Black lines indicate mutations isolated in the suppressor screen.

A *unc-44* termination mutations *ox685*, *ox832*, *ox833*



unc-44 termination splice mutation *ox686*



B *unc-44* construct for *kin-20* rescue

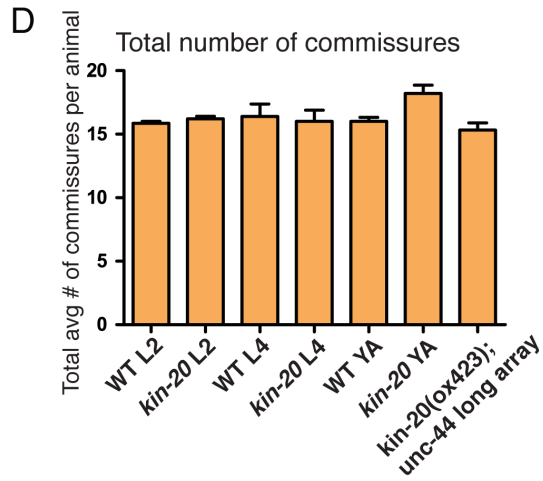
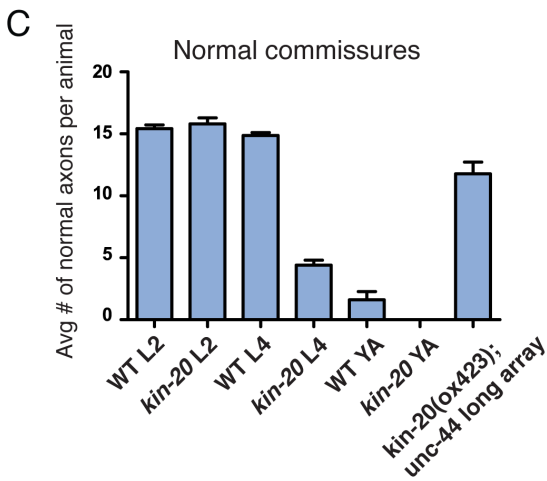
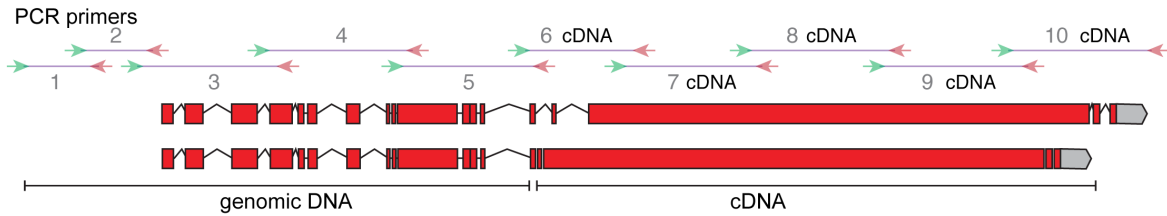


Figure S5. *unc-44* termination mutations and rescue construct related to Figure 5.

(A) **Above**, three *kin-20(ox423)* suppressor mutations were found in the polyA signal sequence. The *unc-44* gene model indicates the 3 major isoforms controlled by polyA site selection. qPCR primer sets are indicated for the short, medium, and long isoforms of *unc-44*, data displayed in Figure 5B and S6.

PolyA site #2 is regulated by CK1 / KIN-20 and termination factors. Nucleotide motifs that coordinate transcription termination and polyadenylation are indicated. The polyadenylation signal sequence AAUAAA is recognized by cleavage and polyadenylation specificity factor (CPSF) and pauses elongation (Chen et al., 2015). Downstream of the signal sequence, the transcript is cleaved and polyadenylated at a CA motif 18-30 nucleotides after the AAUAAA motif (Porrúa and Libri, 2015). The GU-rich sequence is recognized by Cleavage stimulation Factor (CstF) complex, which binds the CPSF complex and promotes efficient cleavage and termination (Kuehner et al., 2011). The U-rich sequence is recognized and bound by both CPSF and CstF components, which enhance cleavage and subsequent polyadenylation (Kuehner et al., 2011; Xiang et al., 2014). Weakened base pairing in this A-U stretch might contribute to the dismounting of the polymerase from the DNA double strand (Sidorenkov et al., 1998).

Alternatively, allosteric changes might be propagated to the RNA polymerase via PCF-11 and the C-terminal interacting domain (CID), or rapid progression of the RNA exonuclease and its helicase may 'torpedo' the RNA polymerase (Kuehner et al., 2011; Richard and Manley, 2009).

Below, another suppressor mutation was identified in a sequence only conserved in nematodes in the intron upstream of polyA site #2. This mutation causes skipping of exon 15 and PolyA site #2, and direct splicing to the giant intron of *unc-44*. Skipping was confirmed by sequencing cDNA using primers oML520 and oML596 (Key resource table).

(B) Expression of UNC-44-Long rescues *kin-20(-)* mutants. The UNC-44-Long rescue construct was generated by PCR products using genomic DNA as a template (PCRs 1-5), or cDNA

template (PCRs 6-10). PCR constructs were injected into *kin-20(ox423)* animals; the overlapping fragments then assembled by homologous recombination to regenerate a complete gene.

(C) The average number of normal GABA motor neuron commissures per animal, control data for Figures 1 and 5. These data illustrate the increasing severity of the *kin-20* axon defect (all stages, ***P<0.001, Welch's t-test). Expressing the long isoform of *unc-44* is sufficient to rescue *kin-20(ox423)* axons (***P<0.001, Welch's t-test); rescue was to nearly wild-type levels in young adults (*P=0.01, Welch's t-test; genotype: *kin-20(ox423); oxEx2085[unc-44(long) minigene]*).

(D) The average total number of GABA motor neuron commissures was scored per animal as a control in our analysis of growth cones, branches, and spindly axons defects as seen in Figures 1C-D & 5C. *kin-20(ox423)* adult animals compared to the wild type are significantly different (*P=0.031, Welch's t-test). Rescued *kin-20(ox423); oxEx2085[unc-44(long) minigene]* adults compared to *kin-20* adults are also significantly different (**P=0.0089, Welch's t-test). Strains used in C and D were the same as in Figures 1 & 5: WT EG1285, *kin-20 (ox423)* EG5202, *kin-20(ox423); oxEx2085[unc-44-long(+)]* EG9248.

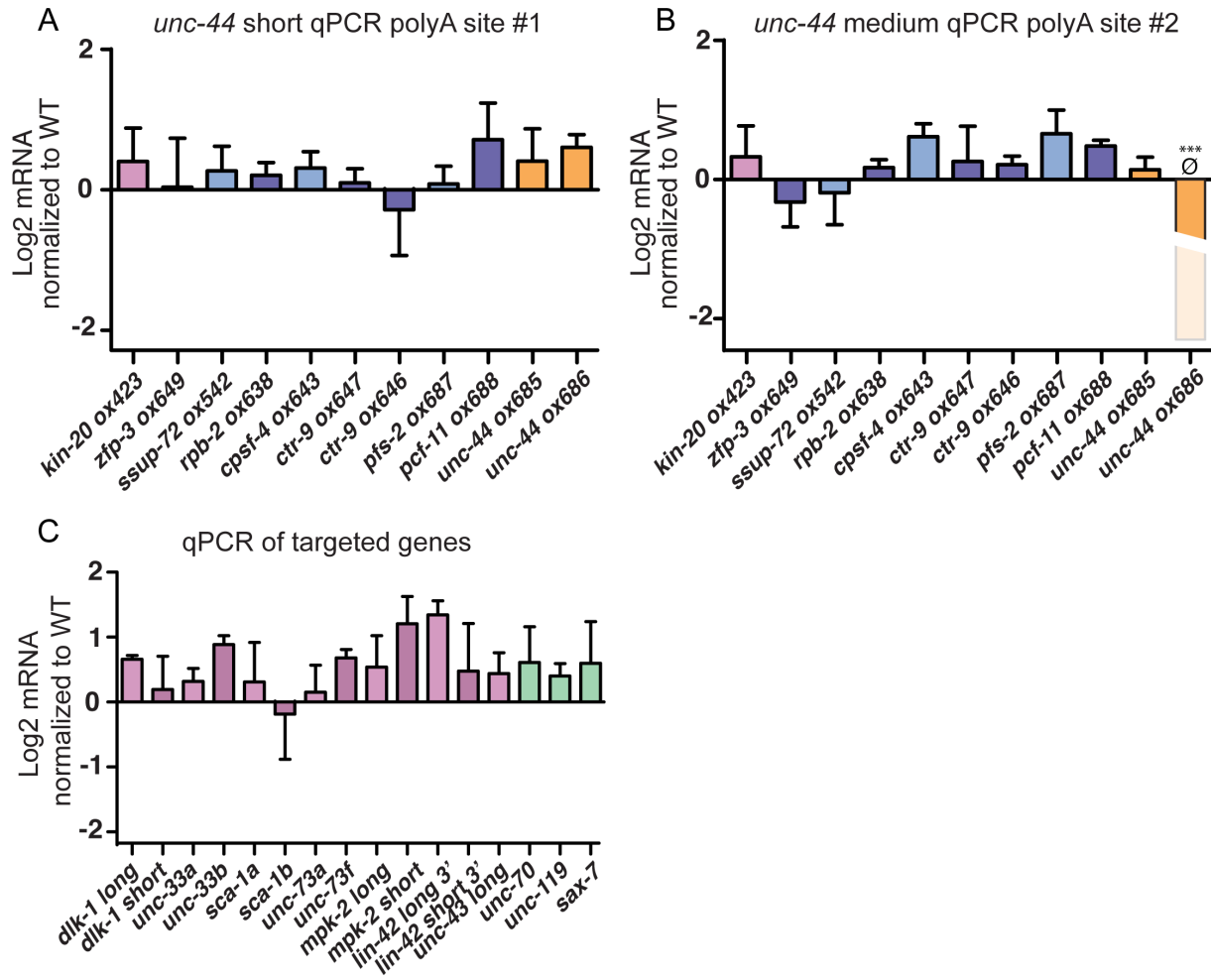


Figure S6. Most *kin-20(ox423)* suppressors do not alter the short or medium isoforms of *unc-44* related to Figure 5.

(A) qPCR of an exon specific to the short isoform of *unc-44* controlled by polyA site #1. No significant differences were found between the suppressors and *kin-20(ox423)* ($p > 0.05$). Each suppressor tested is in a *kin-20(ox423)* background in (A, B). The zero level is wild-type, all samples are normalized to the wild type and the housekeeping gene, *rpl-18* (A, B, C).

(B) qPCR of an exon specific to the *unc-44* medium isoform controlled by polyA site #2. *unc-44(ox686)* does not have a detectable level of the *unc-44* medium transcript and is significantly different from the wild type ($***p < 0.001$). No significant differences were found between the remaining suppressors and *kin-20(ox423)* ($p > 0.05$).

(C) Candidate qPCR screening for isoform level changes in *kin-20(ox423)* vs. wild-type animals. No candidate genes assayed are significantly different ($p > 0.05$).

Comparisons for A-C were made with Dunnett's multiple comparison test.

Tissue	Promoter	<i>kin-20</i> gene	Plasmid ID	Injection mix	# injected P0s	Stable arrays?	Rescue?
Hypodermis	Pdpy-7	pML75 cDNA	pML77	pML77 1ng/ul pML90 1ng/ul pbluescript 98ng/ul	12	NO	NO
Muscle	Pset-18 (pSAM162)	pML75 cDNA	pML78	pML78 1ng/ul pML90 1ng/ul pbluescript 98ng/ul	8	NO	NO
Ubiquitous	Pdpy-30	pML75 cDNA	pML79	pML79 2ng/ul ccGFP 30ng/ul pbluescript 68ng/ul	4	YES	YES
Pan-neuronal	Psnt-1 (pCFJ284)	pML75 cDNA	pML80	pML80 1ng/ul ccGFP 1ng/ul pbluescript 98ng/ul	8 injected kin-20 (<i>ok505</i>)	YES	YES
Hermaphrodite germline	Ppie-1 (pCFJ461)	pML68 gDNA	pML81	pML81 2ng/ul MosSCI mix pbluescript	6	NO	NO
Sperm	Pspe-11 (pCM 1-44)	pML68 gDNA	pML83	pML81 2ng/ul MosSCI mix pbluescript	9	NO	NO

Table S1. Tissue-specific rescue of *kin-20* mutants related to Figure S3.

kin-20(ox423) animals were injected with different promoters expressing *kin-20* cDNA in different tissues. Strains also expressed soluble GFP in GABA neurons. Injected animals were assayed for any non-Unc progeny. The only constructs that were able to form stable transgenic lines were those that could also rescue the uncoordinated phenotype, that is, ubiquitous expression, and pan-neuronal expression. This result suggests that fertility or array formation in *kin-20* nulls is so low, a rescue construct is necessary to maintain a line.

<i>C. elegans</i> Gene name	Mutation	± 5 amino acids	<i>C. elegans</i> amino acid	human gene name	human amino acid	yeast gene name	yeast amino acid	Position (ce10)	Allele name	Strain name
<i>kin-20</i>	revertant	RDSKH Q HIAAYR	stop344 coding AA	CK1delta	Q163	Hrr25	R163	X:15272337- 15272335	—	lost
<i>kin-20</i>	revertant	RDSKH Q HIAAYR	stop344 coding AA	CK1delta	Q163	Hrr25	R163	X:15272337- 15272335	—	lost
<i>kin-20</i>	revertant	RDSKH Q HIAAYR	stop344 coding AA	CK1delta	Q163	Hrr25	R163	X:15272337- 15272335	—	EG9092
<i>kin-20</i>	revertant	RDSKH Q HIAAYR	stop344 coding AA	CK1delta	Q163	Hrr25	R163	X:15272337- 15272335	—	EG9100
<i>kin-19</i>	Ctc→Ttc	QAKQK L MTWDF	L300F	CK1alph a	L301	Hrr25	L293	III:4084893	<i>ox689</i>	EG9070
<i>ssup-72</i>	aTg→aAg	NMNRS M EAHGI	M21K	SSU72	M20	Ssu72	M23	II:6777095	<i>ox633</i>	EG9106
<i>ssup-72</i>	tCt→tTt	IESYG S GNQVK	S39F	SSU72	T38	Ssu72	T41	II:6777193	<i>ox542</i>	EG8338
<i>ssup-72</i>	gGa→gAa	QVKMP G PTV DK	G47E	SSU72	G46	Ssu72	G49	II:6777217	<i>ox632</i>	EG9074
<i>ssup-72</i>	caT→caA	QNGLL H MVDRN	H85Q	SSU72	H83	Ssu72	Q86	II:6777403	<i>ox634</i>	EG9107
<i>ssup-72</i>	gAt→gTt	NIDIE D NAEEA	D145V	SSU72	D143	Ssu72	D146	II:6777630	<i>ox631</i>	EG9065
<i>pinn-1</i>	Gt→Tt	—	5' splice donor	PIN1	—	Ess1	—	II:2888833	<i>ox640</i>	EG9073
<i>pinn-1</i>	gTa→gAa	CLHLL V KHDGS	V57E	PIN1	V62	Ess1	I67	II:2888685	<i>ox641</i>	EG9099
<i>pinn-1</i>	N/A	LAKQF S DCSSA	S109L	PIN1	S111	Ess1	S118	II:2887299	<i>ox827</i>	EG9082
<i>pcf-11</i>	tTt→tAt	DYDAL F ARKIV	F83Y	PCF11	F92	Pcf11	F82	III:5025619	<i>ox688</i>	EG9067
<i>cpsf-4</i>	aTc→aAc	CPLRH I DGEKA	I74N	CPSF4	I60	Yth1	I57	IV:12093124	<i>ox645</i>	EG9109
<i>cpsf-4</i>	Gga→Aga	GLCKK G DQCEF	G93R	CPSF4	G79	Yth1	N78	IV:12093068	<i>ox644</i>	EG9085
<i>cpsf-4</i>	aaA→aaT	FCEPM K TLDYE	K106N	CPSF4	K92	Yth1	K91	IV:12093027	<i>ox643</i>	EG9095
<i>pfs-2</i>	cGa→cAa	SPEGK R LITGC	R158Q	WDR33	R148	Pfs2	R107	II:14358964	<i>ox687</i>	EG9089
<i>ctr-9</i>	gGa→gAa	VWTLI G NLHFA	G601E	CTR9	G572	Ctr9	N621	III:9494540	<i>ox647</i>	EG9079
<i>ctr-9</i>	Gaa→Aaa	HFAK N EWMPAQ	E609K	CTR9	E580	Ctr9	E629	III:9494563	<i>ox646</i>	EG9103
<i>ctr-9</i>	gaA→gaT	HFAK N EWMPAQ	E609D	CTR9	E580	Ctr9	E629	III:9494565	<i>ox826</i>	EG9084
<i>cdc-73</i>	cAg→cTg	GIVTI-frameshift	I194 3' splice acceptor	CDC73	—	Cdc73	—	IV:4044726(ce11)	<i>ox831</i>	EG9091
<i>zfp-3</i>	58 base deletion	tgcaga—gattat	deletion, frameshift	na	—	na	—	X:1441625- 1441567	<i>ox654</i>	EG9071
<i>zfp-3</i>	gT→gA	—	splice donor	na	—	na	—	X:1446482	<i>ox649</i>	EG9090
<i>zfp-3</i>	Cag→Tag	FRSAP Q AAPAP	Q305stop	na	—	na	—	X:1441768	<i>ox650</i>	EG9068
<i>zfp-3</i>	Cag→Tag	FRSAP Q AAPAP	Q305stop	na	—	na	—	X:1441768	<i>ox652</i>	EG9104
<i>zfp-3</i>	Cag→Tag	RRTGR Q NLSI	Q74stop	na	—	na	—	X:1442573	<i>ox648</i>	EG9105
<i>zfp-3</i>	Gt→Ct	—	splice donor	na	—	na	—	X:1444918	<i>ox651</i>	EG9069

<i>C. elegans</i> Gene name	Mutation	± 5 amino acids	<i>C. elegans</i> amino acid	human gene name	human amino acid	yeast gene name	yeast amino acid	Position (ce10)	Allele name	Strain name
<i>zfp-3</i>	3 kb deletion	PCR only	deletion,	na	—	na	—	na	<i>ox807</i>	EG9093
<i>rpb-2</i>	tCg→tTg	NQIYL S KPTHW	S101L	POLR2B	S94	Rpb2	T98	III:4939912	<i>ox639</i>	EG9064
<i>rpb-2</i>	Tac→Cac	LALMAY I SVGS	Y537H	POLR2B	Y531	Rpb2	C564	III:4941264	<i>ox638</i>	EG9098
<i>rpb-2</i>	gTc→gGc	MAYIS V GSLPE	V540G	POLR2B	V534	Rpb2	V547	III:4941274	<i>ox635</i>	EG9094
<i>rpb-2</i>	aTg→aGg	KLRRQ M DIIVS	M600R	POLR2B	M594	Rpb2	G602	III:4941501	<i>ox637</i>	EG9108
<i>rpb-2</i>	aTc→aAc	RQMD I VSEVS	I603N	POLR2B	I597	Rpb2	I6604	III:4941510	<i>ox636</i>	EG9081
<i>cdk-8</i>	Gga/Aga	MMQQP G PSGY	G511R	motif in SON DNA binding protein	G407 in SON	?	?	I:8705436	<i>ox853</i>	EG9078
<i>unc-44</i>	taaAtaaa→ taaGtaaa	—	PAS #2	ANK2, ANK3	—	?	—	IV:5987450	<i>ox685</i>	EG9088
<i>unc-44</i>	taaAtaaa→ taaGtaaa	—	PAS #2	ANK2, ANK3	—	?	—	IV:5987462 (ce11)	<i>ox832</i>	EG9066
<i>unc-44</i>	taaAtaaa→ taaCtaaa	—	PAS #2	ANK2, ANK3	—	?	—	IV:5987462 (ce11)	<i>ox833</i>	EG9087
<i>unc-44</i>	ttAAAAa→ ttTTGaa	—	conserve d intron	ANK2, ANK3	—	?	—	IV:5987182- 5987184	<i>ox686</i>	EG9097
Unverified hits										
<i>pinn-1</i>	caaTtt→ caaGttt	—	intronic, intron #2	PIN1	—	Ess1	—	II:2888818	<i>ox642</i>	EG9077
<i>zfp-3</i>	tgaGttt→ tgaAttt	—	intronic	na	—	na	—	X:1441533	<i>ox653</i>	EG9101
<i>swd-2.2*</i>	Cat/Tat	NNQT C HIAEFS	H292Y	WDR82	divergent	Swd2	divergent	IV:7775613	<i>ox691</i>	EG9080
<i>nrd-1*</i>	cCt/cTt	SLLTQ P QILAK	P323L	SCAF8	unconser ved region	Nrd1	?	I:4601489	<i>ox554</i>	EG9078
<i>f13d11.10</i> <i>*ncRNA?</i>	ion torrent							no relevant mutation found		EG9080
?	ion torrent							no relevant mutation found		EG9102
?	ion torrent							no relevant mutation found		EG9096

Table S2 *kin-20(ox423)* suppressor mutants generated in our ENU mutagenesis screen related to Table 1. 'na', not applicable. Sequences from "ion torrent" were of low quality. * The *nrd-1* mutation was found with the *cdk-8* mutation in strain EG9078; the *cdk-8* mutation was confirmed and is likely to be the relevant mutation in this strain. * The *swd-2.2* mutation was found with the *f13d11.10* ncRNA mutation in strain EG9080; neither mutation was confirmed. No relevant mutations were found in EG9102 or EG9096, because of poor quality sequence data.

gene name	allele name	mutation	± 5 amino acids	<i>C. elegans</i> amino acid	strain name	verified by	verification strain	new allele
<i>rpb-2</i>	<i>ox638</i>	Tac→Cac	LALMAYISVGS	Y537H	EG9098	cross to <i>kin-20(ox505)</i>	EG8964	N/A
<i>ssup-72</i>	<i>ox542</i>	tCt→tTt	IESYGS ^R GNQVK	S39F	EG8338	array OE, or cross to <i>kin-20(ox505)</i>	lost, or EG8967	N/A
<i>pfs-2</i>	<i>ox687</i>	cGa→cAa	SPEGK ^R LITGC	R158Q	EG9089	CRISPR	EG9916	<i>ox838</i>
<i>cdk-8</i>	<i>ox853</i>	Gga/Aga	MMQQP ^G PSGY	G511R	EG9078	CRISPR	EG9915	<i>ox840</i>
<i>cdc-73</i>	<i>ox831</i>	cAg→cTg	3' splice acceptor	I194-frameshift	EG9091	CRISPR	EG9917	<i>ox856</i>
<i>nrd-1</i>	<i>ox554</i>	cCt/cTt	SLLTQ ^P QILAK	P323L	EG9078	no CRISPR	unverified	N/A
<i>pcf-11</i>	<i>ox688</i>	tTt→tAt	DYDAL ^F ARKIV	F83Y	EG9067	no CRISPR	unverified	N/A
<i>swd-2.2</i>	<i>ox691</i>	Cat/Tat	NNQTCH ^I AIEFS	H292Y	EG9080	no CRISPR	unverified	N/A
<i>kin-19</i>	<i>ox689</i>	Ctc→Ttc	QAKQK ^L MTWDF	L300F	EG9070	no CRISPR	unverified	N/A

Table S3. Suppressor strain verification related to Table 1 & Table S2.

Single-allele suppressors were verified by reproducing the ENU-induced allele by CRISPR. The SapTrap CRISPR approach was used to regenerate *pfs-2*, *cdk-8*, and *cdc-73* alleles (see Methods). *pfs-2*, *cdk-8*, and *cdc-73* were crossed to *kin-20(ox423)* to confirm suppression. CRISPR alleles for *nrd-1*, *pcf-11*, and *swd-2.2* eluded us and remain unverified (white). We did not confirm *kin-19* because it is of minor interest. N/A, not applicable.

Candidate gene	Common name	Reason for interest
unc-44	ankyrin	alternative 3' isoforms, required for axon maturation, neuronal
kin-20	casein kinase 1 delta	regulates ankyrin, alternative 3 isoforms, neuronal
unc-5	netrin	guidance protein with alternative 3' isoform
hmp-1	alpha catenin	neuronal adherens junction protein with alternative 3' isoforms
cnb-1	Calcineurin B	alternative 3' isoforms
sca-1	sarco-endoplasmic reticulum Ca[2+] ATPase	alternative 3' isoforms
rga-6	Rho GTPase activating protein 6	alternative 3' isoforms
rep-1	Rab escort protein 1	Neuronal protein with alternative 3' isoform
unc-70	beta spectrin	binds ankyrin, neuronal cytoskeletal protein, alternative splicing
apl-1	amyloid precursor protein (APP)	Neuronal, NO alterative 3' isoform
spc-1	alpha spectrin	non-neuronal cytoskeletal protein
sax-7	L1CAM	binds ankyrin, cell adhesion receptor IG superfamily, alternative 5' ends
mek-1	Map kinase kinase	activates JNK, axon regeneration
pmk-3	p38 mitogen-activated protein kinase	downstream of dlk-1 in axon regeneration pathway, alternative 5' ends
unc-34	VASP homolog	axon guidance protein with alternative 3' isoforms
unc-33	CRMP	binds ankyrin, neuronal polarity, alternative 3' UTRs
unc-119	UNC119	neuronal, phenocopies kin-20 and unc-44
unc-69	SCOC	neuronal, axon guidance, alternative 3' isoforms
lin-42	Period	circadian protein target of CK1, alternative 3' isoforms
ncx-2	sodium/calcium exchanger 1 isoform B	alternative 3' isoforms
stn-1	syntrophin	neuronal, NO alterative 3' isoform
erp-1	endophilin B1	neuronal, alternative 3' isoforms
mpk-2	mitogen activated protein kinase	predicted downstream of RTKs, alternative 3' isoforms
nab-1	neurabin/spinophilin	neuronal F-actin interactor, possible alternative 3' isoforms
spas-1	spastin	neuronal AAA ATPase, microtubule binding and severing
unc-76	FEZ family (fasciculation and elongation; zeta-1)	neuronal, fasciculation, axon outgrowth, alternative 3' isoforms
dyn-1	dynamain	neuronal, alternative 3' isoforms
unc-43	CAMKII	neuronal, alternative 3' isoforms

hipr-1	Huntington interacting protein	neuronal, alternative 3' isoforms
shn-1	SHANK (SH3/ankyrin domain scaffold protein)	neuronal, alternative 3' isoforms
nrx-1	neurexin	neuronal, alternative 5' isoforms
dlk-1	dual-leucine zipper kinase	axon regeneration master regulator, alternative 3' isoforms
dct-1	DAF-16/FOXO Controlled, germline Tumor affecting	alternative 3' isoforms
unc-73	TRIO	Rho / Rac GEF, neuronal, 5' and 3' alt. isoforms

Table S5. qPCR candidate screen related to Figures 5 & S6.

qPCR was performed on the wild type and *kin-20(ox423)* mutants to determine if additional genes other than *unc-44* long were differentially expressed in the mutant. Genes were selected for reasons indicated in the table: alternative poly(A) site usage, known neuronal or synaptic function, as well as controls.